NASr-21-(07)

MEMORANDUM
RM-5110-NASA
DECEMBER 1966

A NUMERICAL GENERAL CIRCULATION EXPERIMENT FOR THE ATMOSPHERE OF MARS

C. B. Leovy and Y. Mintz

PREPARED FOR:
NATIONAL AERONAUTICS AND SPACE ADMINISTRATION

The RAND Corporation
SANTA MONICA • CALIFORNIA

RAND RESEARCH BRIEF
THE RAND CORPORATION
1700 Main St., Santa Monica, Calif.

December 1966 RB-5110

RM-5110-NASA, A Numerical General Circulation Experiment for the Atmosphere of Mars, C. B. Leovy and Y. Mintz, RAND Memorandum, December 1966, 51 pp.

PURPOSE: To describe a numerical experiment to simulate the general circulation of the atmosphere of Mars.

THE MODEL: The dynamical model used was Mintz and Arakawa's two-level primitive equation model, which had already demonstrated its ability to simulate the gross features of the general circulation pattern of the earth. The most important problem in adapting the model to Mars was the specification of the heating functions, since these generate and maintain the circulation. Based mainly on recent studies of the Martian atmosphere and spectrum, it was assumed that the atmosphere was composed entirely of CO_2 and had an initial surface pressure of 5 millibars. Factors taken into account included heating effects of absorption of solar radiation by the atmosphere and by the ground, exchange of infrared radiation between atmospheric layers and between the atmosphere and the ground, conduction into the ground, convective exchange between the ground and the atmosphere, convective transfer between atmospheric layers, and latent heat release due to carbon dioxide condensation at the ground.

THE NUMERICAL EXPERIMENT: Calculation was started from the initial condition of a resting isothermal atmosphere with a temperature of 200°K. The initial ground temperature was taken to be the same. The subsolar point was initially put at 0° longitude and 24.8° south latitude, corresponding to the southern hemisphere summer solstice. The mass of solid CO_2 on the ground was assumed initially to be zero.

FINDINGS: The first possibly important feature indicated by the model was the development of a fluctuating wave regime in the winter hemisphere. These upper-level waves had rapid initial growth rates, and their initial phase speeds corresponded reasonably well with the theoretical speed for a barotropic Rossby wave. A large amplitude diurnal tide was also noted. Perhaps of greatest interest, however, was the condensation of CO_2 to form a winter polar ice cap whose width was close to the maximum width of the observed Mars ice cap.

FUTURE PLANS: An attempt will be made to improve the physical model by reformulating the lower boundary conditions, changing the parameterization of the surface convective heat flux, and considering the effect of clouds on the radiative heating.

BACKGROUND: This RAND study for NASA was motivated by interest in the wind systems on Mars, arising from proposed exploration missions, and by the ability to simulate the circulation of planetary atmospheres by numerical integration of the governing physical equations. (See also RM-5017-NASA, Radiative Convective Equilibrium Calculations for a Two-layer Mars Atmosphere, May 1966.)

AG

MEMORANDUM
RM-5110-NASA
DECEMBER 1966

A NUMERICAL GENERAL CIRCULATION EXPERIMENT FOR THE ATMOSPHERE OF MARS

C. B. Leovy and Y. Mintz

This research is supported by the National Aeronautics and Space Administration under Contract No. NASr-21. This report does not necessarily represent the views of the National Aeronautics and Space Administration.

The RAND Corporation
1700 MAIN ST. • SANTA MONICA • CALIFORNIA • 90406

PREFACE

The experiment reported here is, in part, a result of RAND's long-time interest in computer models of atmospheric dynamics. The goal in this effort was to simulate the global circulation of Mars by application of basic dynamical equations. This Memorandum should be of interest to those concerned with the Mars atmosphere in general, and in particular to persons concerned with atmospheric parameters for Mars lander missions.

ABSTRACT

A numerical model for simulating the general circulation of the atmosphere of Mars is described and preliminary results from an initial experiment are given. The experimental conditions correspond to the northern hemisphere winter solstice on a planet, in the orbit of Mars, having an atmosphere composed entirely of CO_2 and an initial surface pressure of 5 mb. The important features indicated by the model are (1) development of a fluctuating wave regime in the winter hemisphere, (2) a large amplitude diurnal tide, and (3) condensation of CO_2 to form a winter polar ice-cap. The preliminary character of this experiment is stressed and some future improvements are proposed.

ACKNOWLEDGMENTS

The authors wish to thank Dr. Gerard de Vaucouleurs for providing the table of albedo values, and Dr. Akio Arakawa for his valuable advice during the preparation of the experiment. We are deeply indebted to the Jet Propulsion Laboratory for providing the computer time for the experiment, and particularly to Charles Campen, Robert McClatchey, and Frank Herron of JPL for their kind cooperation. Programming of the experiment was carried out by Mr. A. B. Nelson of RAND, and we have benefited from the advice of Mr. Daniel Sabsay during the programming phase. We also wish to acknowledge the support of NASA under Task Order Contract NASr-21(07).

CONTENTS

I. INTRODUCTION

Interest in the wind systems on Mars, arising from proposed exploration missions to the planet, and the ability to simulate the circulation of planetary atmospheres by numerical integration of the governing physical equations have motivated this study.

Recent investigations, by Kaplan, Münch, and Spinrad and by Kliore and his co-workers, have provided new estimates of the mass and composition of the Mars atmosphere. We use these new estimates, together with the known size, surface gravity, rotation period, axial tilt, eccentricity of orbit, and solar constant for Mars. We assume that the surface is level; that is, that there are no large-scale mountains on the planet. Albedo variations according to a tabulation prepared for us by G. de Vaucouleurs have been taken into account, but through an inadvertent transposition of coordinates, those actually used in the experiment do not correspond precisely with de Vaucouleurs' values (see footnote on p. 8).

The dynamical model we use is the two-level primitive equation model of Mintz and Arakawa. This model has already demonstrated its ability to simulate the gross features of the general circulation of the earth's atmosphere. The calculations were done on the IBM 7094 computer at the Jet Propulsion Laboratory, Pasadena. Only preliminary results from the first of several contemplated numerical experiments for Mars are discussed here.

II. THE GOVERNING PHYSICAL EQUATIONS AND NUMERICAL MODEL

When only the hydrostatic approximation is made, the governing equations of fluid motion reduce to the so-called primitive equations, and $\sigma \equiv (p - p_T)/(p_S - p_T)$ can be used as the vertical coordinate, where p is pressure and p_S and p_T are, respectively, pressures at the lower and upper boundaries of the domain (Phillips, 1957). The equations are the horizontal momentum equation,

$$\frac{\partial}{\partial t}(\pi \underset{\sim}{V}) = -\nabla \cdot (\pi \underset{\sim}{\underset{\sim}{V}}\underset{\sim}{V}) - \frac{\partial}{\partial \sigma}(\pi \dot{\sigma} \underset{\sim}{V}) - 2\Omega \sin \underset{\sim}{k} \times (\pi \underset{\sim}{V}) - [\nabla(\pi \Phi) - (\Phi - bRT)\nabla \pi] - \pi \underset{\sim}{F};$$

the thermodynamic energy equation,

$$\frac{\partial}{\partial t}(\pi T) = -\nabla \cdot (\pi \underset{\sim}{V} T) - \frac{\partial}{\partial \sigma}(\pi \dot{\sigma} T) + c_p^{-1} bRT \frac{Dp}{Dt} + c_p^{-1} \pi \dot{h};$$

and the pressure tendency equation

$$\frac{\partial \pi}{\partial t} = -\int_0^1 \nabla \cdot (\pi \underset{\sim}{V})\, d\sigma - (\pi \dot{\sigma})_{\sigma=1},$$

which follows directly from the continuity equation.

In these equations, $\pi \equiv (p_S - p_T)$, $\underset{\sim}{V}$ is the horizontal velocity, and ∇ is the horizontal gradient operator; Ω is the planetary rotation rate, φ the latitude, Φ the geopotential, R the gas constant, $\underset{\sim}{F}$ the frictional force per unit mass, T the temperature, c_p the specific heat at constant pressure, $\dot{h}$ the rate of heat accession per unit mass, and $b \equiv [\sigma + (p_T/\pi)]^{-1}$, and $\underset{\sim}{k}$ is the vertical unit vector.

The variables carried by the model are T and the two components of $\underset{\sim}{V}$ evaluated at the two levels $\sigma = 1/4$ (level 1) and $\sigma = 3/4$ (level 3), together with the pressure variable, π. The average height of level 1 is approximately twelve kilometers and the average height of level 3 is

approximately 3 kilometers. The vertical truncation requires certain modeling assumptions for the vertical variations of T and $\underset{\sim}{V}$; these assumptions are that $\underset{\sim}{V}$ and the potential temperature, $T(p_s/p)^{\kappa}$, vary linearly with σ ($\kappa \equiv R/c_p$).

To evaluate the right-hand sides of these equations, three auxiliary equations are required. These are: the equation for the geopotential,

$$\Phi(\sigma) = \int_{\sigma}^{1} bRT \, d\sigma,$$

which follows from the hydrostatic equation and the assumption that the surface of Mars is level; the equation for the substantial derivative of pressure (Dp/Dt),

$$\frac{Dp}{Dt} = \sigma \left(\frac{\partial \pi}{\partial t} + \underset{\sim}{V} \cdot \nabla\pi\right) + \pi\dot{\sigma},$$

which is a direct consequence of the relationship between p, σ, and π; and the equation for the substantial derivative of σ (denoted by $\dot{\sigma}$),

$$\pi\dot{\sigma} = \int_{0}^{\sigma} \nabla \cdot (\pi\underset{\sim}{V}) \, d\sigma - \sigma \frac{\partial \pi}{\partial t}.$$

The value of $(\pi\dot{\sigma})$ at the lower boundary, $(\pi\dot{\sigma})_{\sigma=1}$, is identically zero except in the case of mass transformation at the ground surface due to CO_2 condensation or sublimation. This case is discussed in the next section, along with the required relationships between $\underset{\sim}{F}$ and $\dot{h}$ and the dependent and independent variables. In the derivation of the pressure tendency equation, p_T was taken as a constant (0.415 mb) so that $\dot{\sigma} \equiv 0$ where $\sigma = 0$.

The finite-difference analogues of the equations are used according to the space differencing scheme of Arakawa (1966b); for a discussion of the principle behind this scheme, see also Arakawa (1966a). The finite-difference representation of the time derivatives is that of Matsuno (1966a,b), which has the property of damping high-frequency gravity waves but leaves all other motions practically unaffected.

The calculation used a spherical grid with horizontal grid intervals of 9 degrees longitude around the planet and 7 degrees latitude from

77° South to 77° North, plus the two poles. This provides values for each variable, at each level, at about 1000 points. The 9-by-7-degree intervals make the zonal and meridional linear scales equal at latitude 39°.

III. APPLICATION OF THE MODEL TO MARS

The most important problem in adapting the model to Mars is the specification of the heating functions, since these generate and maintain the circulation. The heating functions depend on the composition and mass of the atmosphere and on the nature of the planet's surface. Based mainly on the results of Kaplan, Münch, and Spinrad (1964) and of Kliore et al. (1965), we assume an atmosphere composed entirely of CO_2 and having an initial surface pressure of 5 mb. We consider the heating effects of absorption of solar radiation by the atmosphere and by the ground, the exchange of infrared radiation between atmospheric layers and between the atmosphere and the ground, conduction into the ground, convective exchange between the ground and atmosphere, and convective transfer between atmospheric layers. In addition, latent heat release due to carbon dioxide condensation at the ground is taken into account. A possibly significant heat budget item that is omitted entirely is the effect of clouds or aerosols in the atmosphere.

The formulation of the heating functions has been described in detail elsewhere (Leovy, 1966), and only a brief discussion and the actual formulas employed are presented here.

The rate of accession per unit mass to the i-th atmospheric layer, $\dot{h}_i$, resulting from the heating processes listed above, is

$$\dot{h}_i = \frac{g}{\Delta p} (\Delta S_i + \Delta F_i + \Delta C_i),$$

where ΔS_i, ΔF_i, and ΔC_i are the differences between the net downward energy fluxes at the top and bottom of the layer arising, respectively, from solar radiation, infrared radiation, and small-scale turbulent convection. The latter is due to all horizontal scales of vertical motion smaller than the horizontal grid interval. The quantity $g/\Delta p$ is the mass of the layer per unit area, where g is the acceleration of gravity, and Δp is the thickness of the layer in pressure units.

The method employed by Houghton (1963) for computing stratospheric heating rates due to CO_2 is used to compute the ΔS_i. The resulting formulas are

$$\Delta S_1 = \left(\frac{r_m}{r}\right)^2 (\sin \alpha)^{1/2}\{389 + (\sin \alpha)^{1/2} + [2006 + 449 \ln (\csc \alpha)]\},$$

for the upper layer, and

$$\Delta S_3 = \left(\frac{r_m}{r}\right)^2 (\sin \alpha)^{1/2}[316 + 550(\sin \alpha)^{1/2}],$$

for the lower layer. In these formulas (r_m/r) is the ratio of Mars' mean distance from the sun to its actual distance, α is the local solar elevation angle, and the units of ΔS_1 and ΔS_3 are ergs/cm^{2}sec. Subscripts 1 and 3 refer, respectively, to the levels at which $\sigma = 1/4$ and $3/4$.

To compute the infrared heating, we assume that the temperature varies linearly with geometric height up to the level of the tropopause ($\sigma = 0$), where $p_T \equiv 0.415$ mb (Leovy, 1966). Above this level the temperature is assumed to be constant with height, and equal to the temperature at $\sigma = 0$ obtained from the linear extrapolation of the temperatures at $\sigma = 1/4$ and $\sigma = 3/4$. In addition, we assume that a thin layer, which can have a large stable or unstable lapse rate, lies between the ground and the rest of the atmosphere. The assumed depth of this layer is not critical; it is taken to be 5 meters.

The transmission functions of Prabhakara and Hogan (1965) are used to evaluate the infrared fluxes. The resulting formulas for the flux differences are

$$\Delta F_1 = -1.473 \times 10^6 Y(T_t) + [1.204T_2 - 349 + 23200T_2^{-1}][T_1 - T_3] - 0.1282 \times 10^6 [Y(T_4) - Y(T_G)],$$

for the upper layer, and

$$\Delta F_3 = -0.455 \times 10^6 Y(T_t) + [1.710T_2 + 195 - 5880T_2^{-1}][T_1 - T_3]$$
$$-1.800 \times 10^6[Y(T_4) - Y(T_G)]$$
$$+ 1.30 \times 10^8 T_4^{-2} \exp(964.1/T_4)[Y(T_4)^2][T_4 - T_G],$$

for the lower layer. Here, in addition to the temperatures T_1 and T_3, and the ground temperature, T_G, which are computed by the model, appear the tropopause temperature, T_t, and the surface air temperature, T_4, obtained by linear extrapolation from T_1 and T_3. The function $Y(T)$ in these expressions is

$$Y(T) = [\exp(964.1/T) - 1]^{-1}.$$

Again, the units of ΔF_1 and ΔF_3 are ergs cm^{-2} sec^{-1}. Temperatures are expressed in degrees Kelvin.

To evaluate the heat balance at the ground, we require the net upward infrared radiation flux at the ground, F_G. The expression for this quantity is

$$F_G = 5.67 \times 10^{-5} - 1.929 \times 10^6 Y(T_G)$$
$$+ [13.2T_2 - 1560 - 18900T_2^{-1}][T_1 - T_3]$$
$$+ 1.30 \times 10^8 T_4^{-2} \exp(964.1/T_4)[Y(T_4)]^2[T_4 - T_G].$$

Convective heat exchange between ground and atmosphere, C_G, is formulated in two ways, depending on whether the difference between the ground temperature, T_G, and the surface air temperature, T_4, is positive or negative. For $(T_G - T_4) > 0$, the surface air layer is assumed to be unstably stratified, and we take

$$C_G = \bar{\rho} c_p U_M (T_G - T_4),$$

where $\overline{\rho}$ is the mean surface air density. The parameter U_M is taken to have a constant value of 26 cm/sec. This value was derived from the observed Mars diurnal surface temperature wave (Leovy, 1966). Because radiative transfer processes dominate the surface heat balance, the value is not very reliable; it constitutes one of the major uncertainties of our experiment. This point is considered in more detail in the final section.

When $(T_G - T_4) < 0$, the surface air layer is assumed to be stably stratified and the convective heat transfer dominated by turbulence induced by the surface wind. Under these conditions,

$$C_G = \overline{\rho} c_p C_h |V_S| (T_G - T_4),$$

where $|V_S|$ is the magnitude of the surface wind, linearly extrapolated from the winds at $\sigma = 1/4$ and $3/4$, and C_h is a drag coefficient for heat transfer having the value 0.010.

Convective heat transfer between levels 1 and 3 is assumed to take place only if the lapse rate determined by T_1 and T_3 is statically unstable. If the lapse rate is unstable, an upward convective heat flux is assumed to take place at a very rapid rate, warming the upper level and cooling the lower level, such that the time constant for adjustment to the adiabatic lapse rate is approximately one computational time step (1/240 of a Mars day, or 6 Mars minutes).

To evaluate upward radiative and convective transfer, the ground temperature, T_G, is required. This is carried as an auxiliary variable in the program, and its rate of change is determined by the heat balance condition at the ground,

$$(1 - A)S_G - F_G - C_G - D_G + L = 0,$$

where A is the albedo of the ground. The albedo values used in this experiment, and shown in Fig. 1,* were prepared for us by Dr. Gerard de Vaucouleurs,** based on his study (1964). In this equation, the heat

*The coordinates were inadvertently used with longitude increasing counterclockwise as viewed from the North Pole. The effect of this was that the sun's longitudinal motion relative to albedo features was the reverse of its actual motion.

**Personal communication.

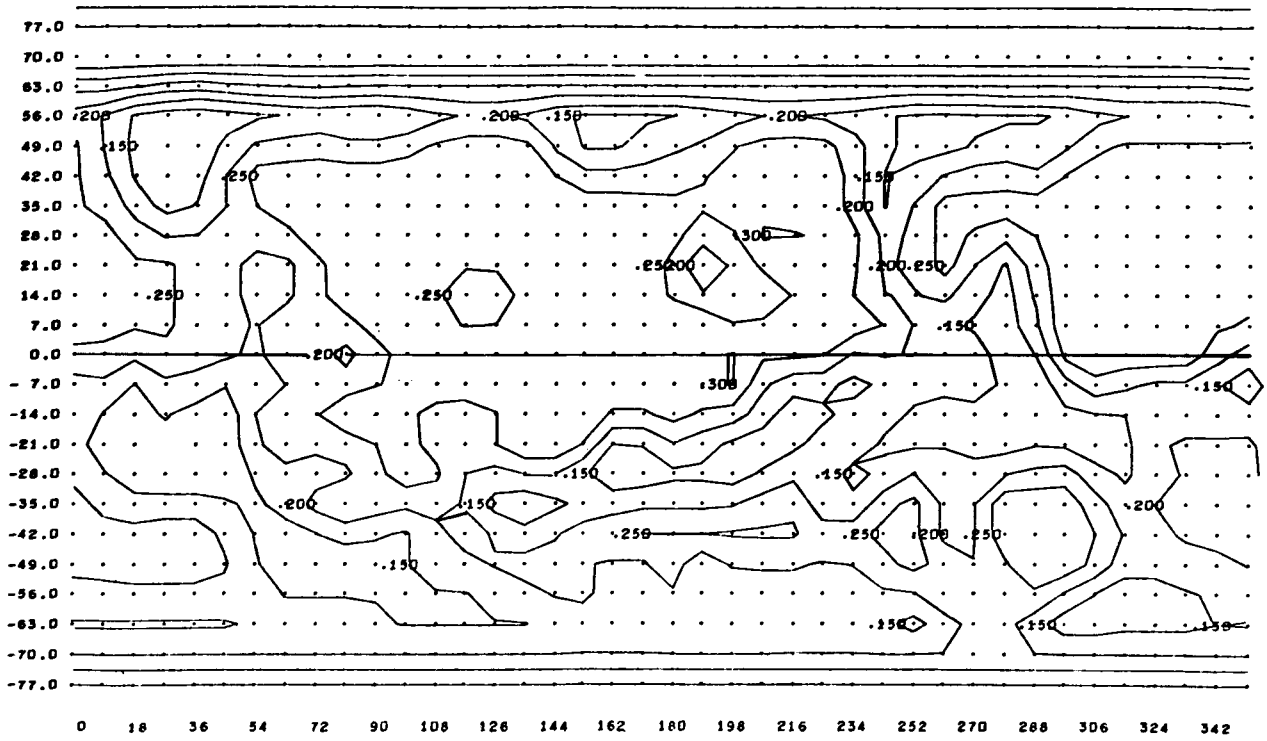

Fig. 1 -- Surface albedo of Mars used in the experiment; grid-point values provided by G. de Vaucouleurs. (Cylindrical projection with even spacing of latitude. Areographic coordinates with North Pole at the top; see footnote, p. 8.)

balance components at the air-ground interface are the downward flux of solar radiation, S_G; the net upward flux of infrared radiation, F_G; the upward convective heat flux from the ground to the air, C_G; conduction of heat downward into the soil, D_G; and latent heat release at the surface, L. The latter is due to CO_2 condensation ($L > 0$), or sublimation ($L < 0$).

When there is no solid CO_2 on the surface, and no condensation or sublimation of CO_2, the surface temperature change is determined by the soil heat flux, D_G. Leovy (1966) has shown that when the major part of the surface temperature variation is periodic with a known period, as is the case for Mars, then D_G can be expressed with satisfactory accuracy in terms of the surface temperature and its time derivative,

$$D_G \approx \rho_s c_s (k_s \omega/2)^{1/2} [0.8(T_G - T_\infty) + 1.2\, \omega^{-1} (\partial T_G/\partial t)],$$

where ρ_s, c_s, and k_s are the density, specific heat, and thermal diffusivity of the soil, and ω is the predominant frequency in the temperature variation; in this case, ω is the diurnal frequency. T_∞ is a temperature at great depth in the soil. In our model, T_∞ is arbitrarily allowed to adjust to T_G with a time constant of 5 days. The parameter $(\rho_s c_s k_s^{1/2})$ is assumed to be the same for the entire planet and has been evaluated from the diurnal surface temperature wave given by Sinton and Strong (1960). The value we use is 8×10^4 ergs cm^{-2} $^oK^{-1}$ sec^{-1}.

The mass of CO_2 condensed on the surface is accounted for in the calculation. Whenever the surface temperature starts to fall below the condensation temperature (143.6°K), or when any condensed CO_2 is already present on the surface, we let $(\partial T_G/\partial t) = 0$, so that the surface temperature remains fixed at 143.6°K; this enables L and the corresponding rate of mass transformation at the surface to be computed as the residual of the terms in the surface heat balance equation. The mass transformation is reflected in the dynamics by allowing a corresponding mass flux through the surface. In other words, the value of L determines the value of $\dot{\sigma}$ at $\sigma = 1$. When solid CO_2 is on the surface, the albedo takes on the value 0.6.

Potential energy produced by the heating functions is converted by the model into kinetic energy. The kinetic energy is dissipated in the model in four ways: by friction at the ground, by vertical shear stresses by lateral diffusion, and by the time differencing scheme.

In the earth's atmosphere, at least in middle and high latitudes, one does not observe large amounts of energy in space scales that are small but still resolvable by the usual finite difference grids. The physical reason for this is not clear. In numerical general circulation experiments, this result can be obtained by dissipating the energy of the high wave numbers by a lateral diffusion term. We have done this in the Mars experiment, using the lateral diffusion coefficient $A = 6 \times 10^4(\Delta s/300)^{4/3}$ m^2/sec, where Δs is the local grid distance in kilometers. This is the diffusion coefficient value used by Mintz (1965) in his experiment simulating the earth's atmosphere.

Surface stress, $\underset{\sim}{\tau}_s$, is accounted for by a drag law formulation,

$$\underset{\sim}{\tau}_s = -\rho C_D |\underset{\sim}{V}_s| \underset{\sim}{V}_s \ .$$

For the drag coefficient, C_D, two values are used: $C_D = 0.9 \times 10^{-3}$ for stable surface air ($T_G \leq T_4$), and $C_D = 3.6 \times 10^{-3}$ for unstable surface air ($T_G > T_4$). Lettau (1959) found that for the earth's atmosphere, C_D varies only slowly with surface roughness when it is defined in terms of the geostrophic surface wind, and the values we use are based on his findings for moderately rough surfaces and stable and unstable conditions.

Parameterization of the momentum exchange between the two atmospheric levels is one of the major uncertainties of our model. We arbitrarily let this exchange be proportional to the vector difference between the velocities at the two levels, with the proportionality constant equal to 2×10^{-7} sec^{-1} when the temperature difference between the two levels corresponds to stable stratification, and equal to 4×10^{-6} sec^{-1} when the difference corresponds to unstable stratification.

IV. THE NUMERICAL EXPERIMENT

The calculation was started from the initial condition of a resting isothermal atmosphere, with a temperature of 200°K. The initial ground temperature was also taken as 200°K. The subsolar point was initially put at 0° longitude and 24.8° South latitude, corresponding to the southern hemisphere summer solstice. The mass of solid CO_2 on the ground was assumed initially to be zero.

Some difficulty was experienced in the vicinity of the south pole. A nearly zonally symmetric one-grid-point oscillation, which damped rapidly away from the pole, was observed. This oscillation evidently arose from a computational instability associated with the special treatment of the polar points in this particular version of Arakawa's finite-difference scheme. Because the heating is concentrated in the southern hemisphere, and has a very strong diurnal variation, an intense tidal flow directly across the pole was generated. In addition, the static stability near this summer pole rapidly became very small, favoring the development of high-frequency gravity waves. The cause of the computational instability may be an aliasing of the gravity waves due to the change in the north-south spacing of the grid next to the pole, although other aspects of the finite-difference treatment of the polar point may also be involved.

In order to control this computational problem, the heating field near the south pole was smoothed in three different ways:

1. During the entire experiment, the albedo was smoothed for the polar point and for the four adjacent grid point latitudes. This had the effect of smoothing the solar radiation received at the ground and the consequent heat flux into the atmosphere. It also eliminated the residual small south polar summer ice cap that appears in de Vaucouleurs' data. This device slowed considerably the growth rate of the polar oscillation.
2. During the first 15 days (Mars days) of the experiment, the atmospheric heating rates over the pole and over the four adjacent grid point latitudes were also smoothed directly,

causing a decrease in the tidal forcing near the pole. This technique further diminished the growth rate of the oscillation.

3. From Day 12 until the conclusion of the experiment on Day 24, direct smoothing of the heating was not used. Instead, the thermal conductivity of the ground at the pole was increased by a factor of five; on the four adjacent grid point latitudes, it was increased by progressively smaller factors. Again the goal was to decrease smoothly the rate of heat input to the atmosphere near the pole. This technique was not as successful in controlling the polar oscillation as the direct smoothing of the heating. There is a 3-day interval--from Day 12 to Day 15--when the two techniques can be compared. Although the problem region in the vicinity of the south pole behaved very differently in the two cases, the close similarity of the flow everywhere else supports our belief that this computational difficulty did not significantly influence the results except in the immediate vicinity of the south pole.

Figure 2 illustrates the growth of the energy during the experiment. The "mean <u>total</u> kinetic energy" is defined by

$$K = \frac{a^2}{4gM} \int_{-\pi/2}^{\pi/2} \cos\varphi \int_0^{2\pi} \left[(p_S - p_T)(\underset{\sim}{V}_1 \cdot \underset{\sim}{V}_1 + \underset{\sim}{V}_3 \cdot \underset{\sim}{V}_3) \right] d\lambda \, d\varphi$$

where M is the total mass of the troposphere and a is the radius of Mars. The "mean <u>zonal</u> kinetic energy" is

$$\bar{K} = \frac{1}{4\pi} \int_{-\pi/2}^{\pi/2} \cos\varphi \, (\bar{\underset{\sim}{V}}_1 \cdot \bar{\underset{\sim}{V}}_1 + \bar{\underset{\sim}{V}}_3 \cdot \bar{\underset{\sim}{V}}_3) \, d\varphi,$$

where the bar operator is defined by

$$\overline{(\quad)} = \frac{1}{2\pi(\bar{p}_S - p_T)} \int_0^{2\pi} (p_S - p_T)(\quad) \, d\lambda,$$

and

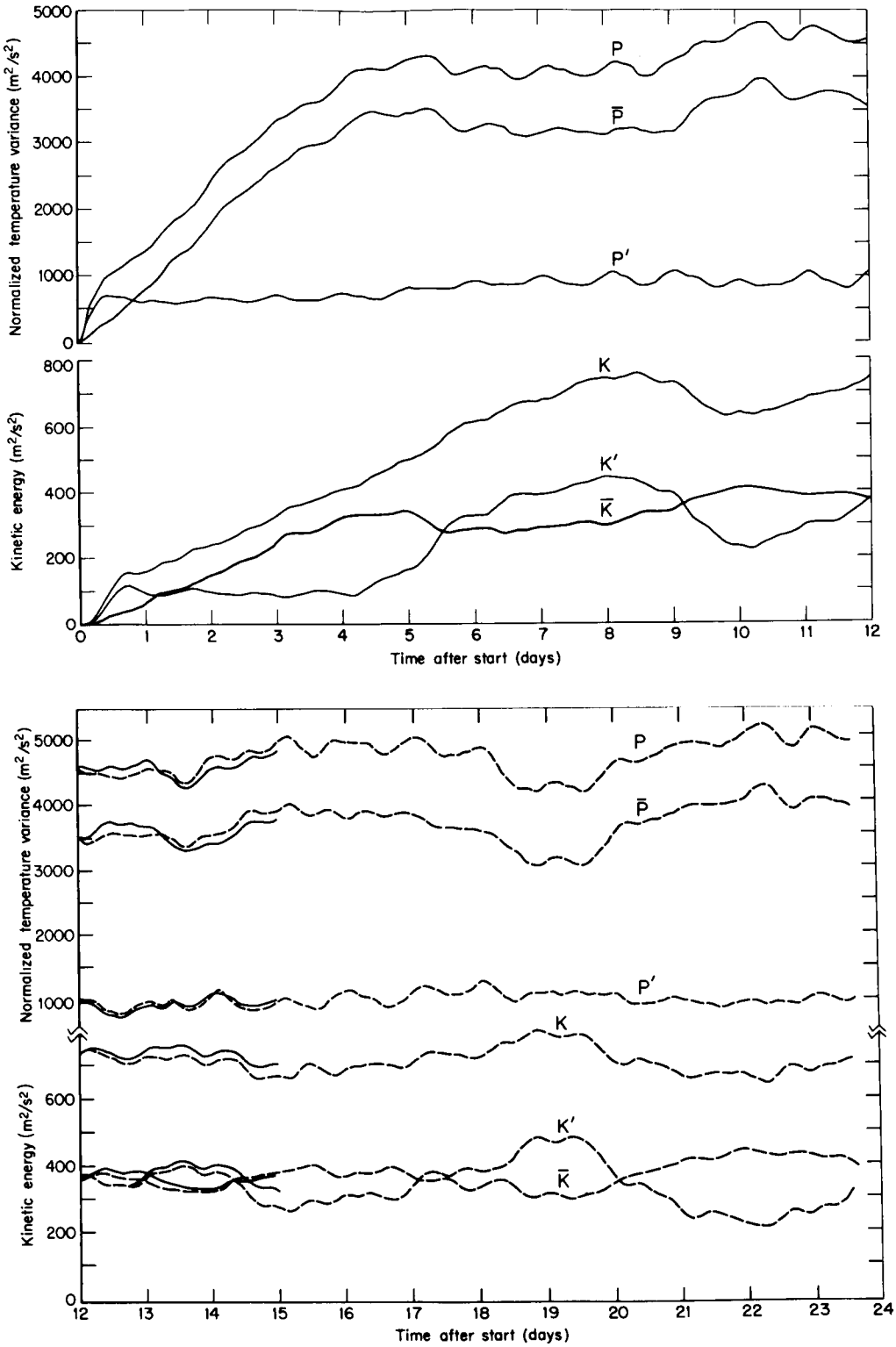

Fig. 2 -- Variation of total, mean, and perturbation components of kinetic energy and normalized temperature variance (see text for exact definitions of these quantities). The solid curves correspond to direct smoothing of the heating near the South Pole; the dashed curves correspond to indirect smoothing by increasing the soil heat capacity near the South Pole.

$$\overline{p}_S = (1/2\pi) \int_0^{2\pi} p_S \, d\lambda .$$

The "mean perturbation kinetic energy" is

$$K' = K - \overline{K} .$$

The integrations are over latitude, φ, and longitude, λ.

Similarly, we show the variance of the temperature from its horizontal mean, normalized so as to yield an approximation to the average available potential energy per unit mass.

The "normalized total temperature variance" is

$$P = \frac{a^2}{2gM} \int_{-\pi/2}^{\pi/2} \cos\varphi \int_0^{2\pi} (p_S - p_T) \left[\frac{(T_1 - \overline{T}_1)^2}{Q_1} + \frac{(T_3 - \overline{T}_3)^2}{Q_3} \right] d\lambda \, d\varphi ,$$

where $$Q_i = 2[\overline{T}_1 (\overline{p_S/p_1})^{\kappa} - \overline{T}_3 (\overline{p_S/p_3})^{\kappa}][R (\overline{p_S/p_i})^{\kappa}]^{-1} ,$$

$\kappa = R/c_p$, and $\overline{T}$ is the global mean temperature for the level. The "normalized zonal temperature variance" is

$$\overline{P} = \frac{1}{2\pi} \int_{-\pi/2}^{\pi/2} \cos\varphi \left[\frac{\overline{(T_1 - \overline{T}_1)^2}}{Q_1} + \frac{\overline{(T_3 - \overline{T}_3)^2}}{Q_3} \right] d\varphi .$$

The "normalized perturbation temperature variance" is

$$P' = P - \overline{P} .$$

The lower three curves in Fig. 2 show, respectively, the mean total kinetic energy, K; the mean zonal kinetic energy, $\overline{K}$; and the mean perturbation kinetic energy, K'. The upper three curves in the figure show, respectively, P, $\overline{P}$, and P'.

The overlap of the curves, from Day 12 to Day 15, illustrates the effect on the energies of the two techniques used for controlling the south polar instability.

Initially there is a rapid growth of the temperature variances and the kinetic energies. These are associated with the diurnal heating and thermally driven diurnal tide. The maximum intensity of the tide occurs during the first day. The mean perturbation kinetic energy during the first 4 days is entirely due to this tide and its higher harmonics. During the first 4 days there is nearly linear growth in both $\overline{P}$ and $\overline{K}$. Between Days 4 and 7, there is a rapid growth in K' and a leveling off, or slight decrease, in $\overline{P}$. This suggests that the disturbances responsible for the increase in kinetic energy are transporting heat toward the winter pole and reducing the meridional temperature gradient. The energy curves further suggest that some kind of statistical equilibrium has been reached by Day 7. The equilibrium is not characterized by a steady state, but, like the earth's atmosphere, is subject to fluctuations between zonal and perturbation kinetic energy as well as to fluctuations of the total kinetic energy. Inspection of the curves shows that the total and the perturbation kinetic energies have a strong positive correlation, but that there is a negative correlation between $\overline{P}$ and $\overline{K}$, on the one hand, and K' on the other. There is a marked 6-day period in the energy fluctuations.

Profiles of zonally averaged wind are shown in Figs. 3 and 4, for both the meridional and zonal components. There is a very intense thermally direct meridional circulation in low latitudes, with rising motion in the southern hemisphere subtropics and descending motion in the northern hemisphere. The zonal winds have an intense westerly jet at the upper levels in mid-latitudes of the winter hemisphere, with weaker easterly winds in the summer hemisphere. The rather noisy character of the profiles at high southern latitudes is in part, at least, a consequence of the computational instability discussed above. Figure 3, for Day 10 of the experiment, corresponds to the phase of the energy fluctuation cycle at which the mean zonal kinetic energy is a relative maximum, while Day 14 corresponds to a relative minimum in mean zonal kinetic energy. On Day 10, when the eddies are relatively weak, the westerly jet is intense with strong lateral shear; on Day 14, the eddies are relatively strong and the jet is weaker and broader.

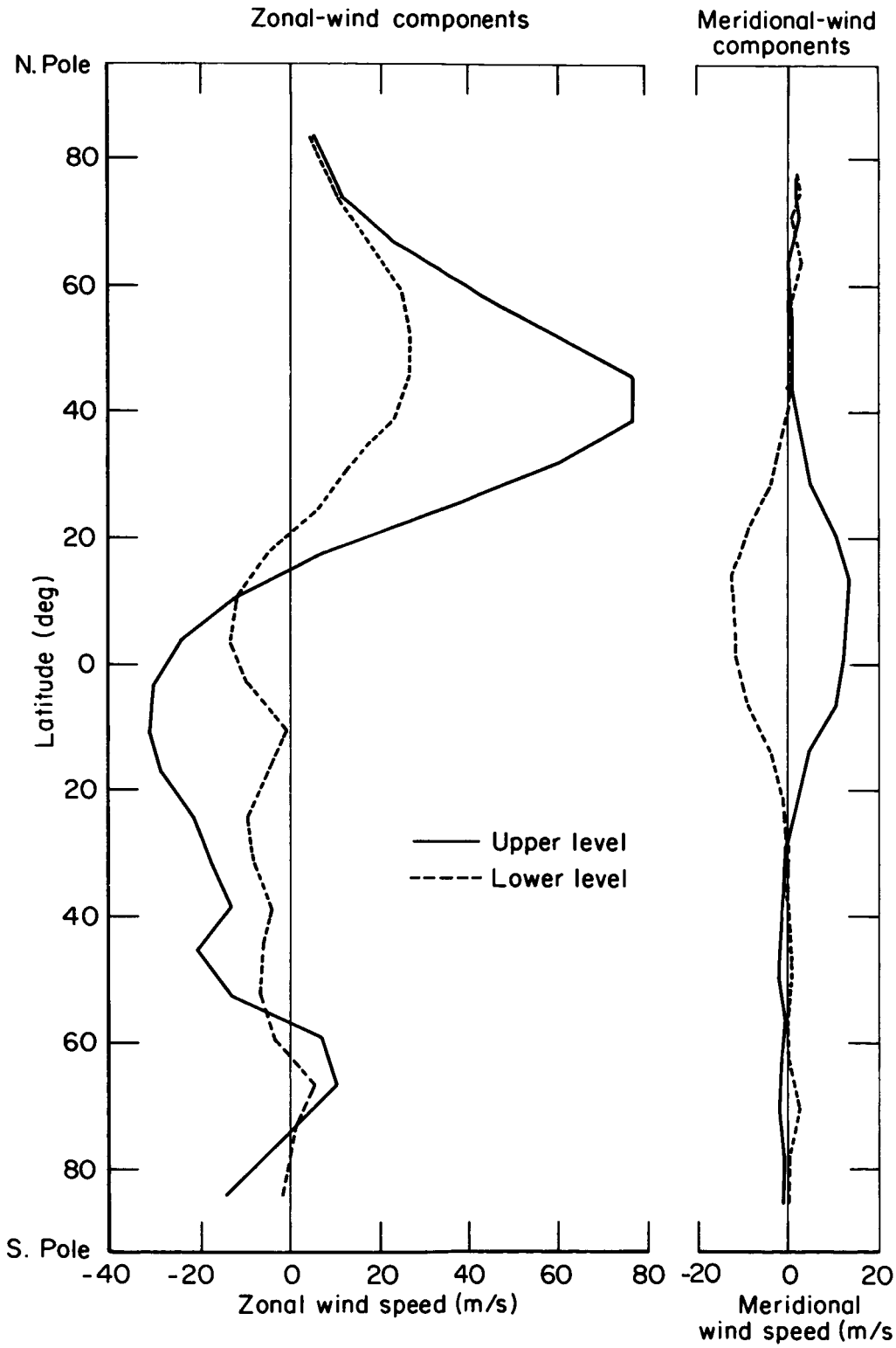

Fig. 3 -- Mean zonal and meridional wind profiles for Day 10. Positive zonal winds are from the west; positive meridional winds are from the south.

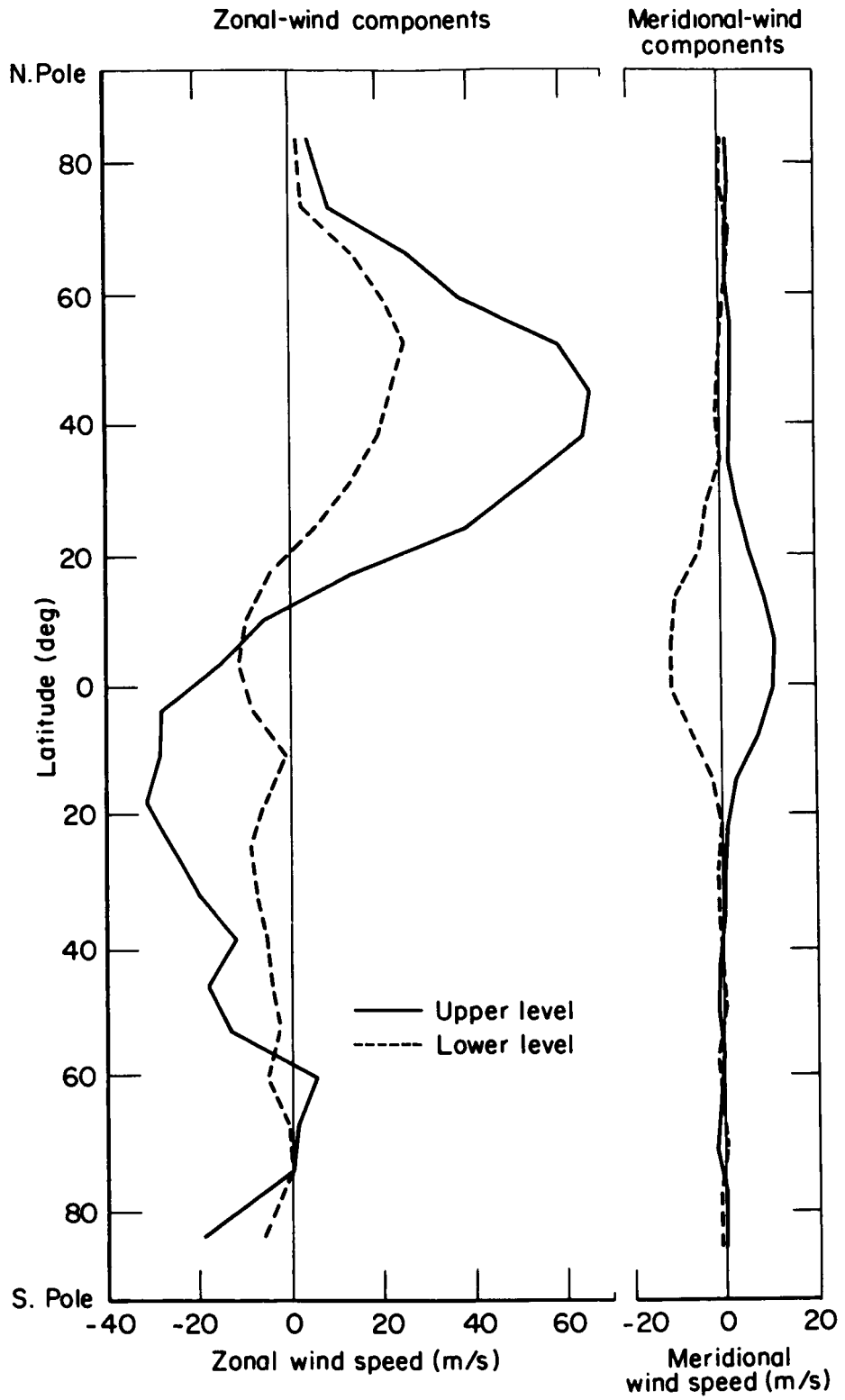

Fig. 4 -- Mean zonal and meridional wind profiles for Day 14.0. Positive zonal winds are from the west; positive meridional winds are from the south.

This characteristic behavior is typical of the same phases during other cycles of the energy fluctuation.

Figures 5 and 6 show meridional profiles of zonally averaged ground and atmospheric temperatures for Day 14. Profiles for other days, subsequent to the intial transient phase of the experiment, are very similar. The temperature profiles computed in this experiment can be compared with similar profiles that were computed without any circulation effects (Leovy, 1966). The ground surface temperature is seen to be almost uninfluenced by the circulation; this is to be expected in view of the very small mass of the atmosphere and its correspondingly poor ability to transport heat. On the other hand, the atmospheric temperatures are noticeably modified by the circulation. The lapse rate in tropical latitudes is reduced by the circulation from nearly adiabatic (which is approximately 5^{o}/km, or 45^{o} between the two levels) to less than half that value. In middle latitudes of the winter hemisphere, the lapse rate is reduced by the circulation from about two-thirds of the adiabatic rate to a nearly isothermal condition.

The circulation reduces the meridional temperature gradients in the atmosphere, especially in the tropics of both hemispheres. No direct comparison can be made to show the effect of the circulation on the temperatures of the atmosphere over the polar cap because, in the calculation without circulation (Leovy, 1966), the atmospheric temperatures were not allowed to fall below the CO_2 frost point, whereas in the circulation experiment no such constraint is put on the atmospheric temperatures.

One of the most interesting features is the development of a CO_2 ice cap (shown by the flat portion of the ground temperature curve in high winter latitudes). This ice cap begins to form during the second day of the experiment and its area is stabilized by the sixth day. Its width is close to the maximum width of the observed Mars ice cap (Slipher, 1962) and is essentially the same as that computed without an atmospheric calculation (Leovy, 1966). In the current experiment, the atmospheric temperatures at the two levels over the ice cap remain near (but are never very much below) the CO_2 vapor pressure equilibrium temperatures, despite the face that radiation cools the air. This is because of the compensating warming produced by the circulation.

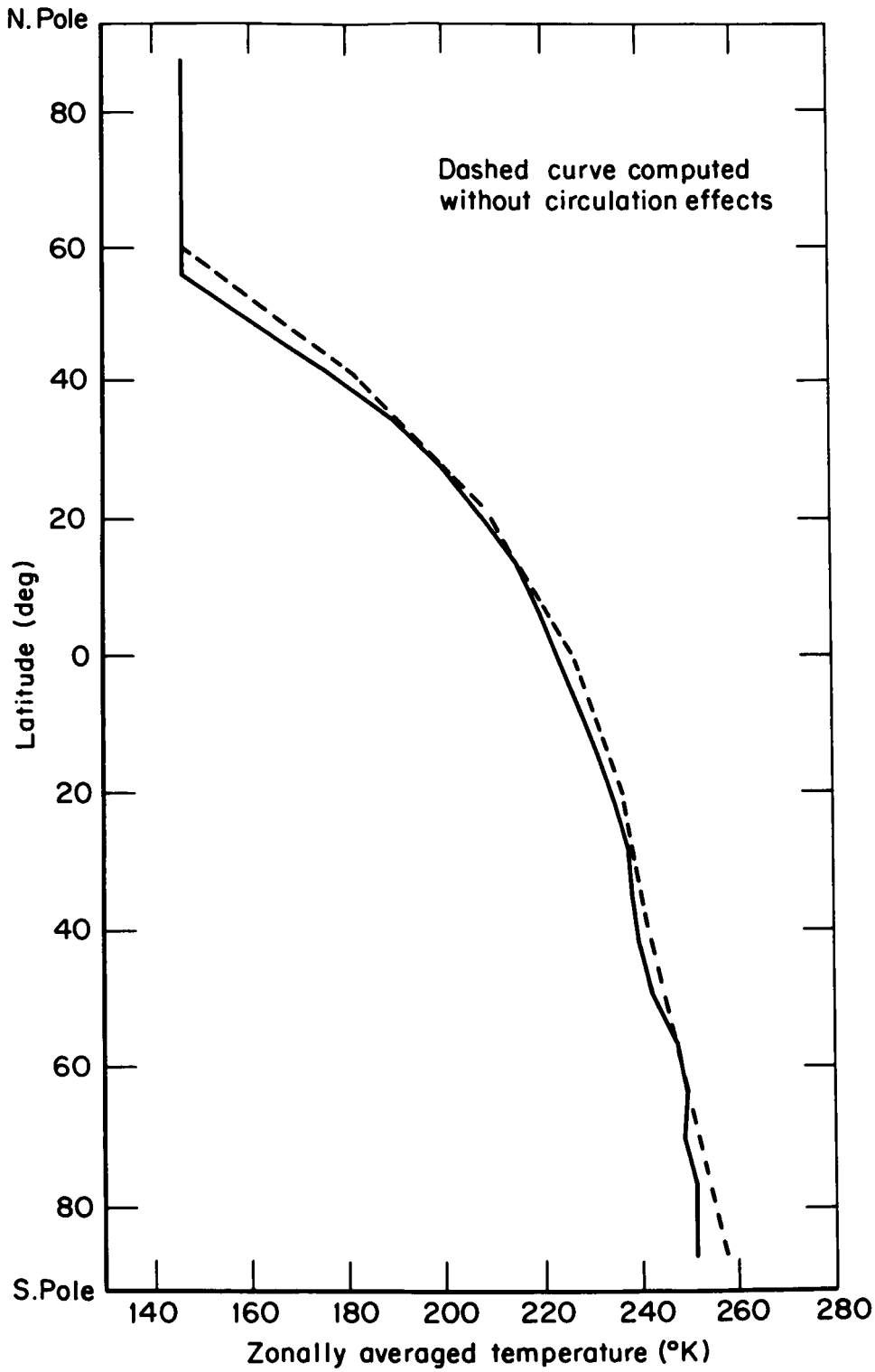

Fig. 5 -- Zonally averaged ground surface temperature; computed by the circulation model for Day 14.0, and computed without circulation effects by a radiative and convective equilibrium model.

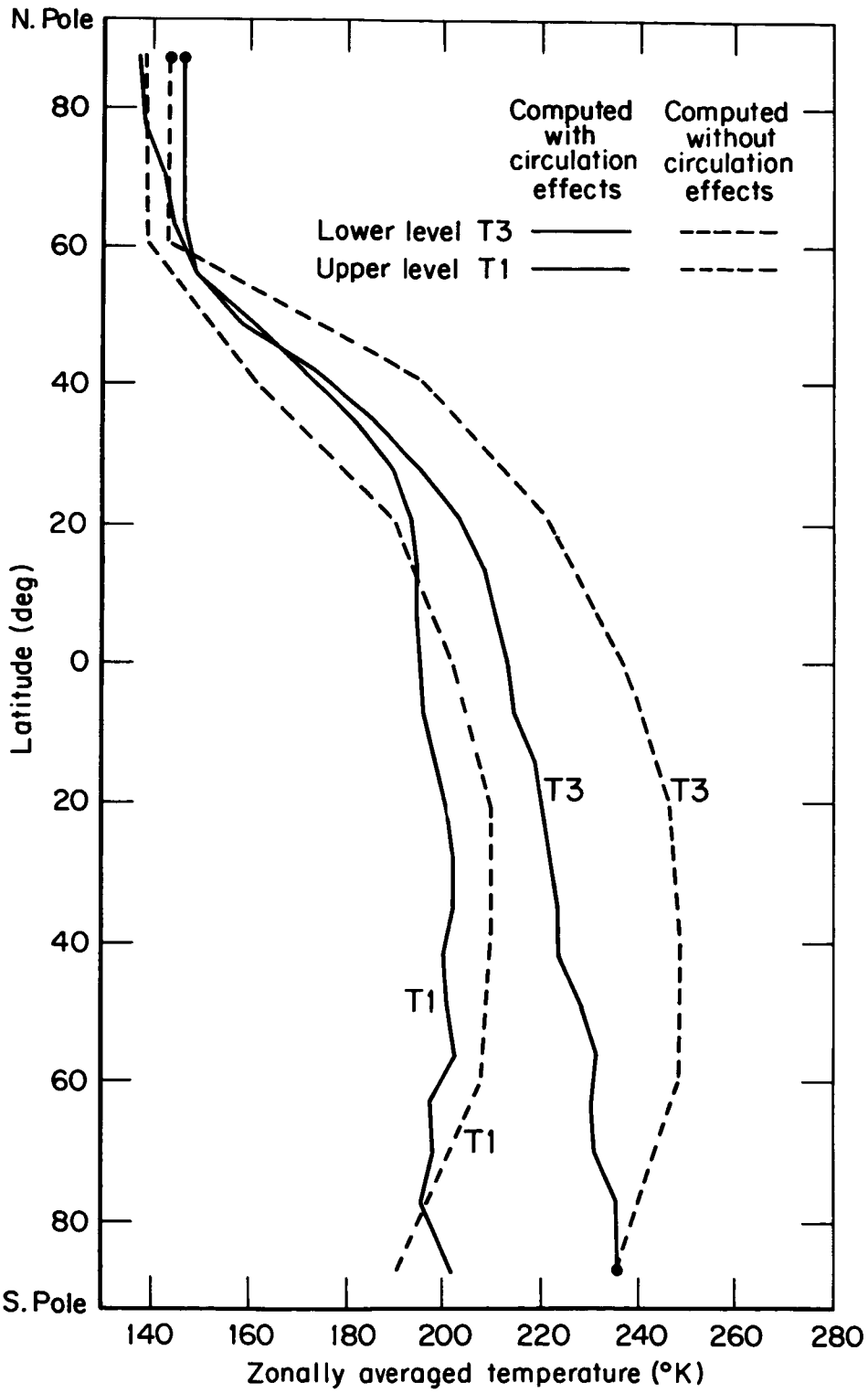

Fig. 6 -- Zonally averaged atmospheric temperatures computed by the model for Day 14.0 and computed without circulation effects by a radiative and convective equilibrium model.

Profiles of surface pressure and surface wind are shown, in Fig. 7, for Days 10, 14, and 22. They show a pressure minimum near the subsolar latitude, a belt of high pressure centered near 35°N, and a polar low. Surface mean zonal winds are not exactly geostrophic, but there is a marked tendency toward geostrophy. The most prominent features are the westerlies in the higher latitudes of the winter hemisphere; the easterlies in the lower latitudes of the winter hemisphere; the narrow belt of westerlies near the equator in the summer hemisphere, produced by the eastward recurving of the flow across the equator; and the predominantly easterly flow over most of the summer hemisphere. The surface pressure drop produced by carbon dioxide condensation in the winter ice cap is clearly shown in the right half of Fig. 7. Formation of the ice cap produces an average drop of 0.01 mb per day in the global mean surface pressure.

The kind of disturbances that begin to dominate in the perturbation part of the temperature variance, and the perturbation kinetic energy after the fourth day of the experiment may best be seen in the upper level temperature field. Figure 8(a-e) shows the development of disturbances in the transition to a wave regime in the winter hemisphere. The maps, at 24-hour intervals starting with Day 3, show the beginning of a wave formation in the region of maximum temperature gradient near areographic longitude 60°. Eventually four waves appear, with initial growth rates such that the amplitude appears to at least double in one day. In the early stages, the waves move eastward with phase speeds from 15 to 30 meters/sec; as they reach the mature stage, however, they tend to stagnate and, in some cases, to retrograde. At later stages of the experiment, wave number three becomes the most prominent, and there is a more confused state of developing short waves moving into and reinforcing stationary mature troughs.

Figure 9(a-c), for Days 18.0, 18.5, and 19.0, illustrates the mature stage of the waves. It also shows the diurnal variation in the upper level temperature. This is most marked in the 180° shift of the broad summer hemisphere warm belt in 12 hours. Figure 10(a-c) shows

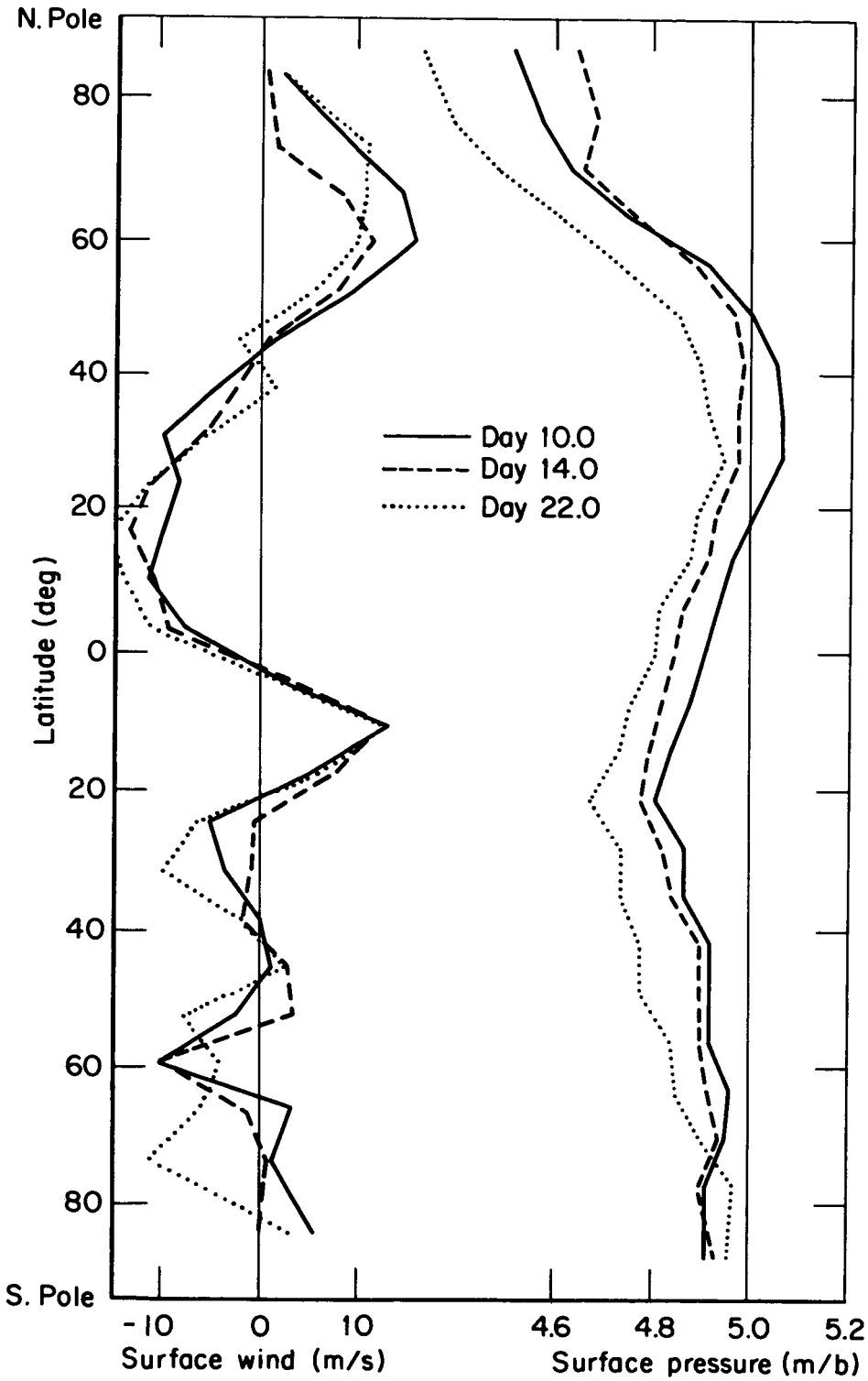

Fig. 7 -- Zonally averaged "surface" wind and surface pressure for three days.

8(a) Day 3.0

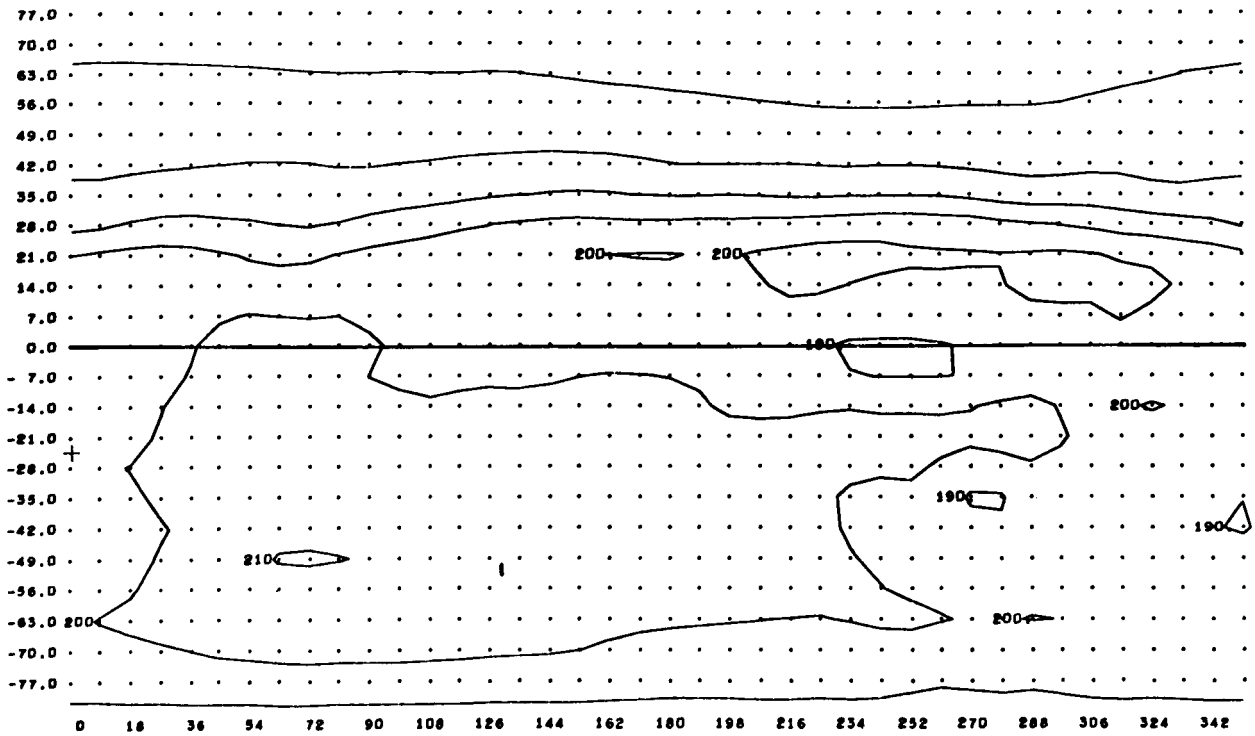

Fig. 8(a,b,c,d,e) -- The upper level temperature field (^{o}K) at 24 hour intervals from Day 3.0 through Day 7.0. Subsolar point is indicated by the (+).

8(b) Day 4.0

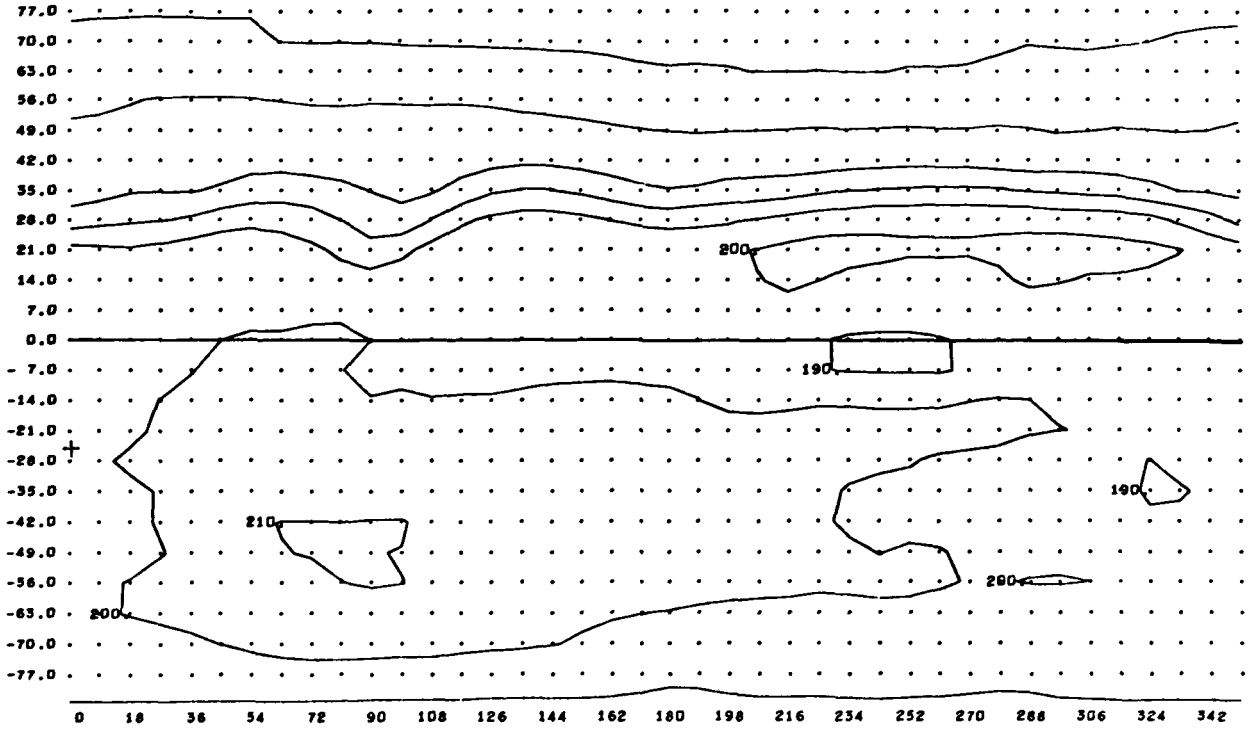

8(c) Day 5.0

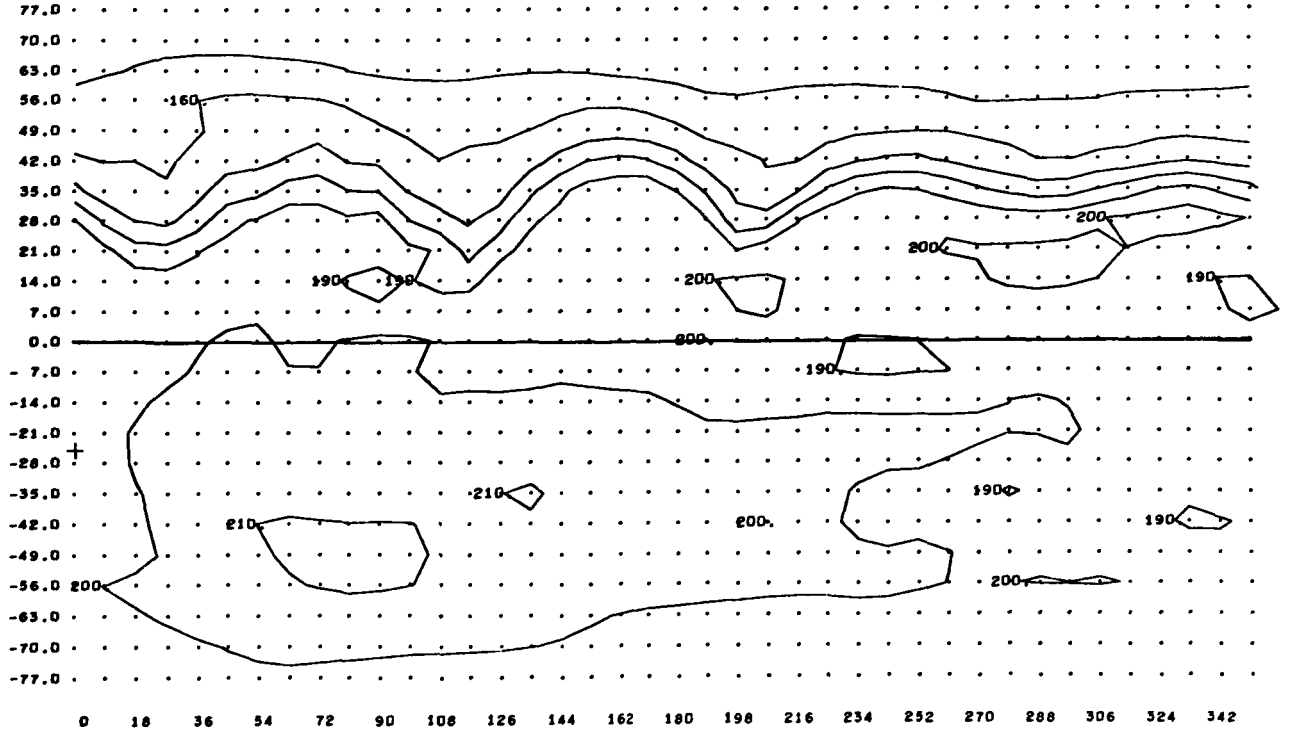

8(d) Day 6.0

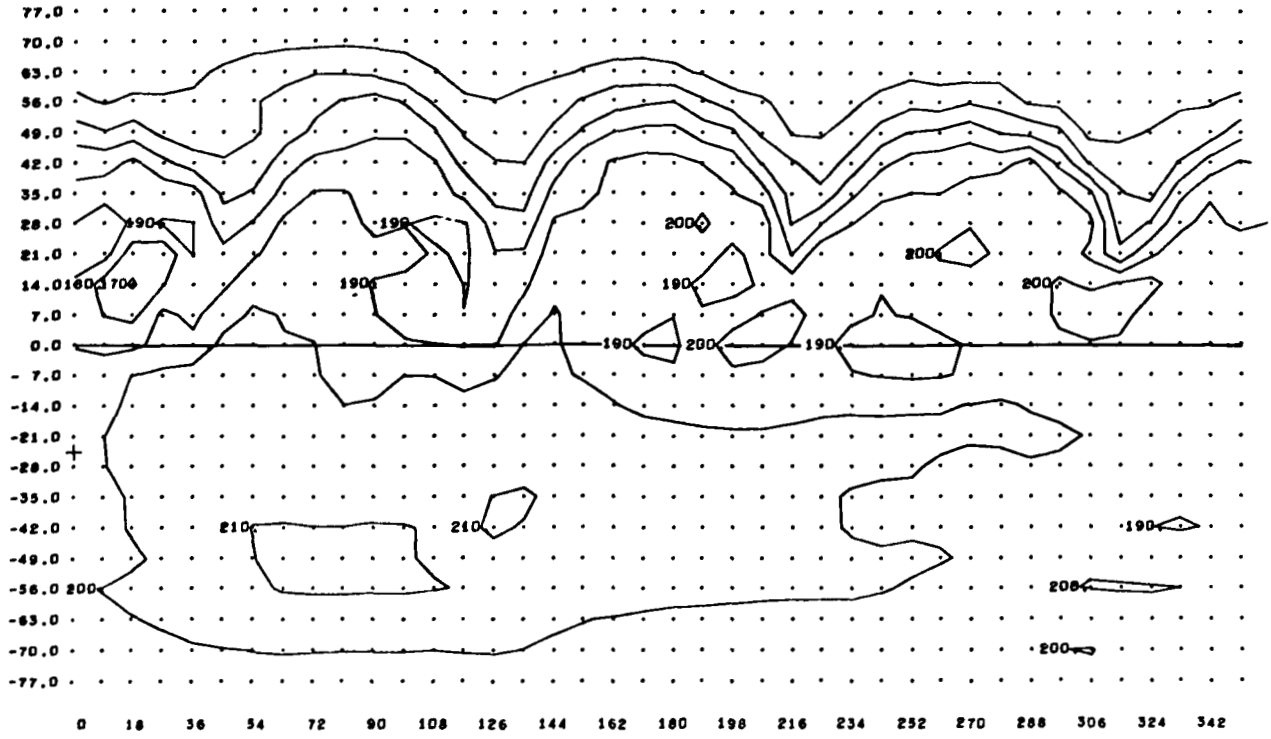

8(e) Day 7.0

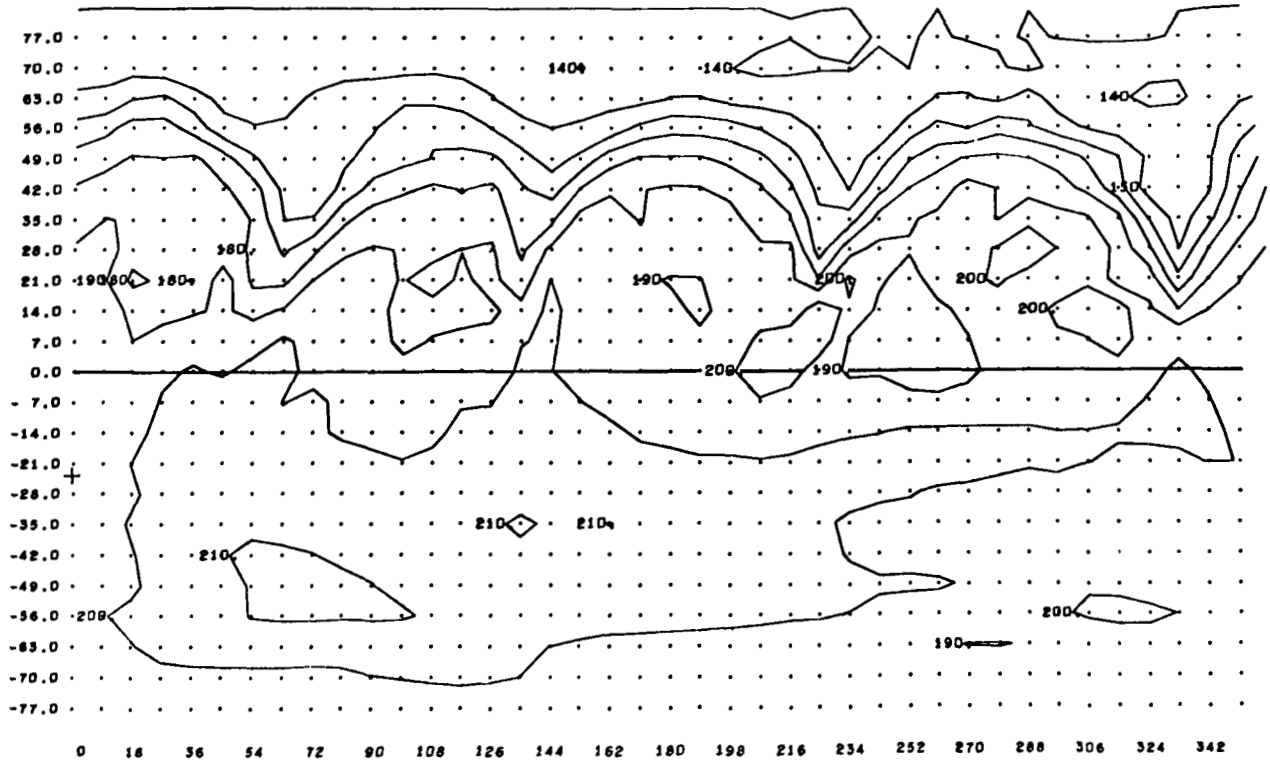

9(a) Day 18.0

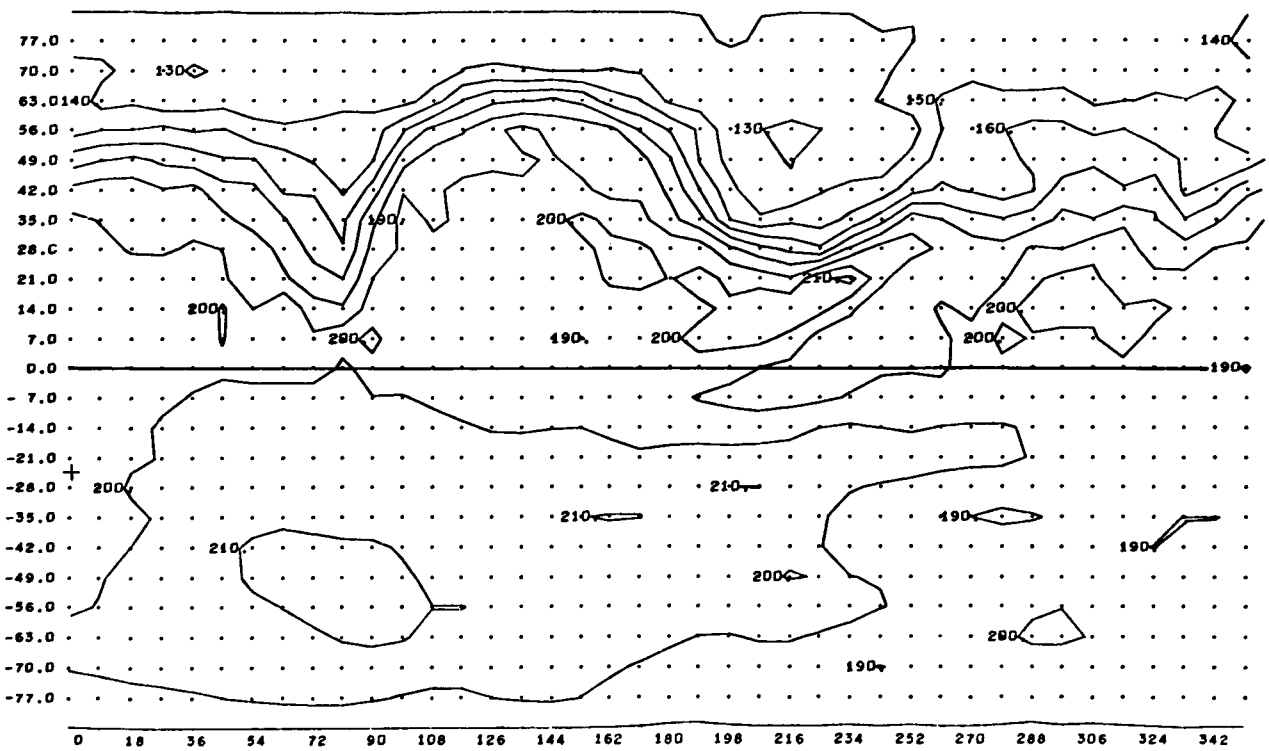

Fig. 9(a,b,c) -- Upper level temperature field (^{o}K) at 12 hour intervals for Days 18.0, 18.5, 19.0. Subsolar point is indicated by the (+).

9(b) Day 18.5

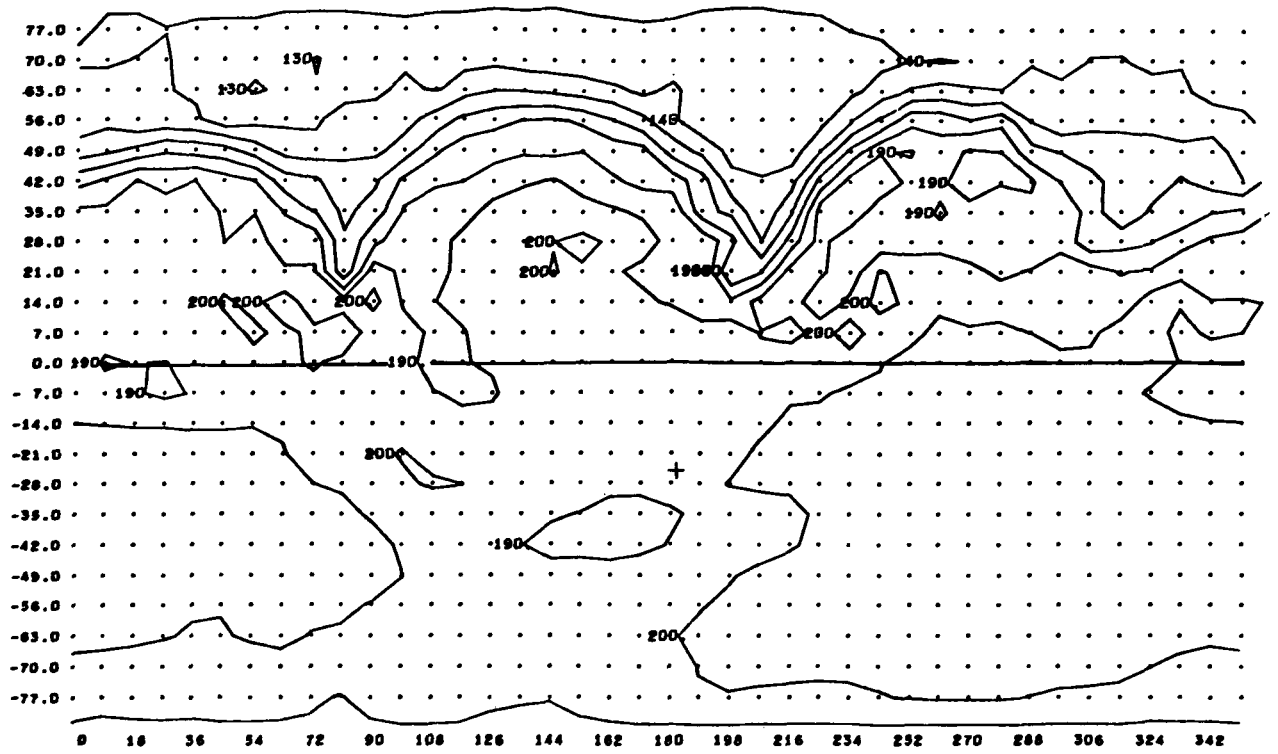

9(c) Day 19.0

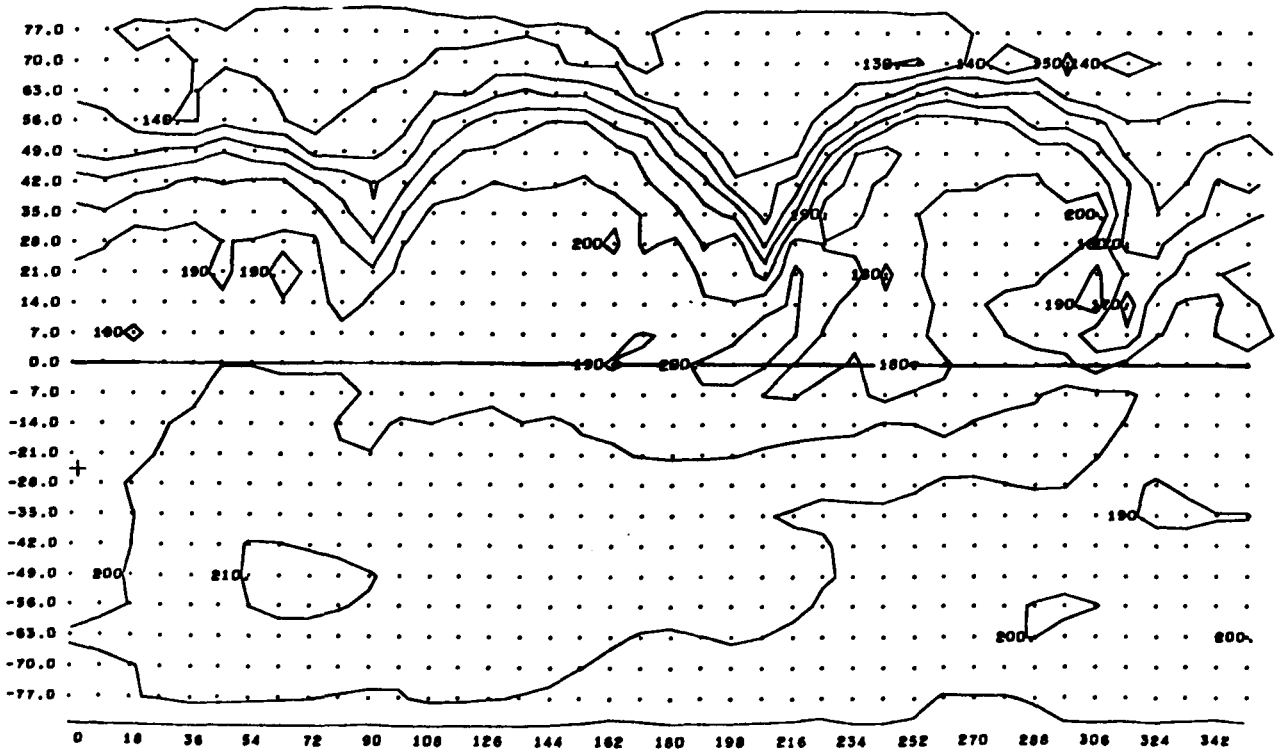

10(a) Day 18.0

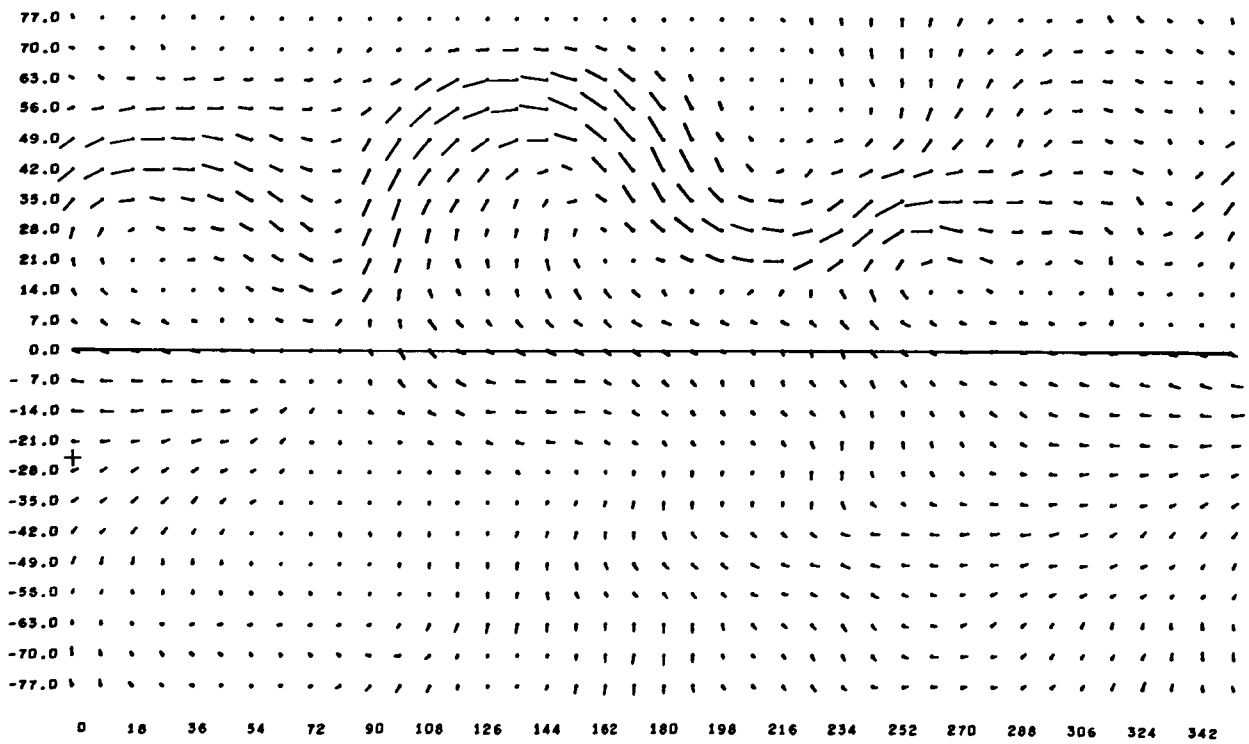

Fig. 10(a,b,c) -- Upper level wind field at 12 hour intervals for Days 18.0, 18.5, and 19.0. The winds blow in the direction toward the dots and the magnitudes are scaled according to the strongest wind on the map which is 146.2 m/s in (a), 162.4 m/s in (b), and 144.1 m/s in (c).

10(b) Day 18.5

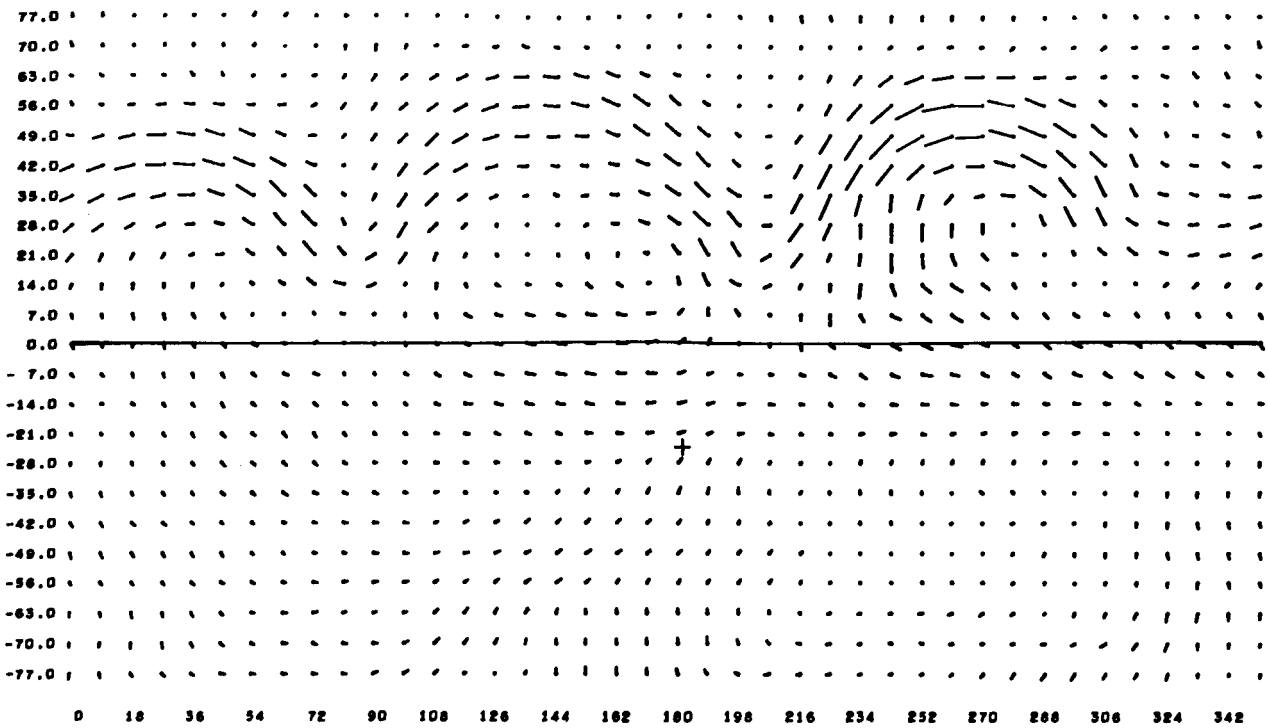

10(c) Day 19.0

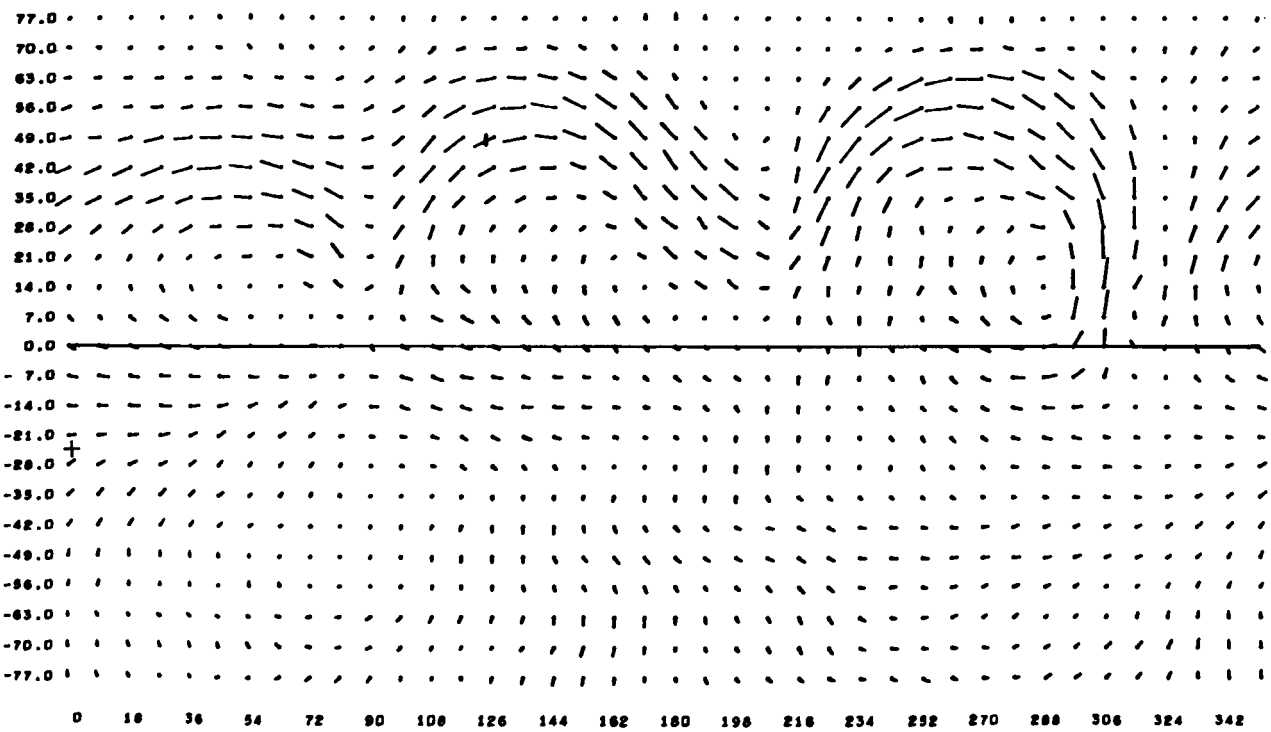

the corresponding upper level wind vectors. In the winter hemisphere, there is close correspondence between the upper level wind and the temperature patterns. The summer hemisphere, however, is dominated by the diurnal tide--with an almost perfect reversal of the winds in 12 hours. The "surface" wind and the surface pressure are shown for the same three times in Figs. 11(a-c) and 12(a-c). The "surface" winds are the winds extrapolated downward from $\sigma = 1/4$ and $\sigma = 3/4$ and should represent winds near the top of a boundary layer. According to data given by Lettau (1959), these winds should be about twice as strong as winds 2 meters above the surface. Both the surface wind and the surface pressure are dominated by the diurnal tide. The high velocity of the surface wind, and the large amplitude of the surface pressure oscillation ($\pm$ 0.35 mb), are probably sensitive to the rate of convective heat exchange between ground to atmosphere. As discussed in the previous section, this rate of heat transfer is large compared with terrestrial experience, and we therefore suspect that the intensity of the computed surface winds in this experiment represents an upper limit for the intensity of the actual large-scale surface winds on Mars.

Lastly, Fig. 13(a-c) shows the ground temperature distributions for the same three times. The limits of the polar ice cap (143.6°K) are close to the printout contour of $T_G = 150°K$.

11(a) Day 18.0

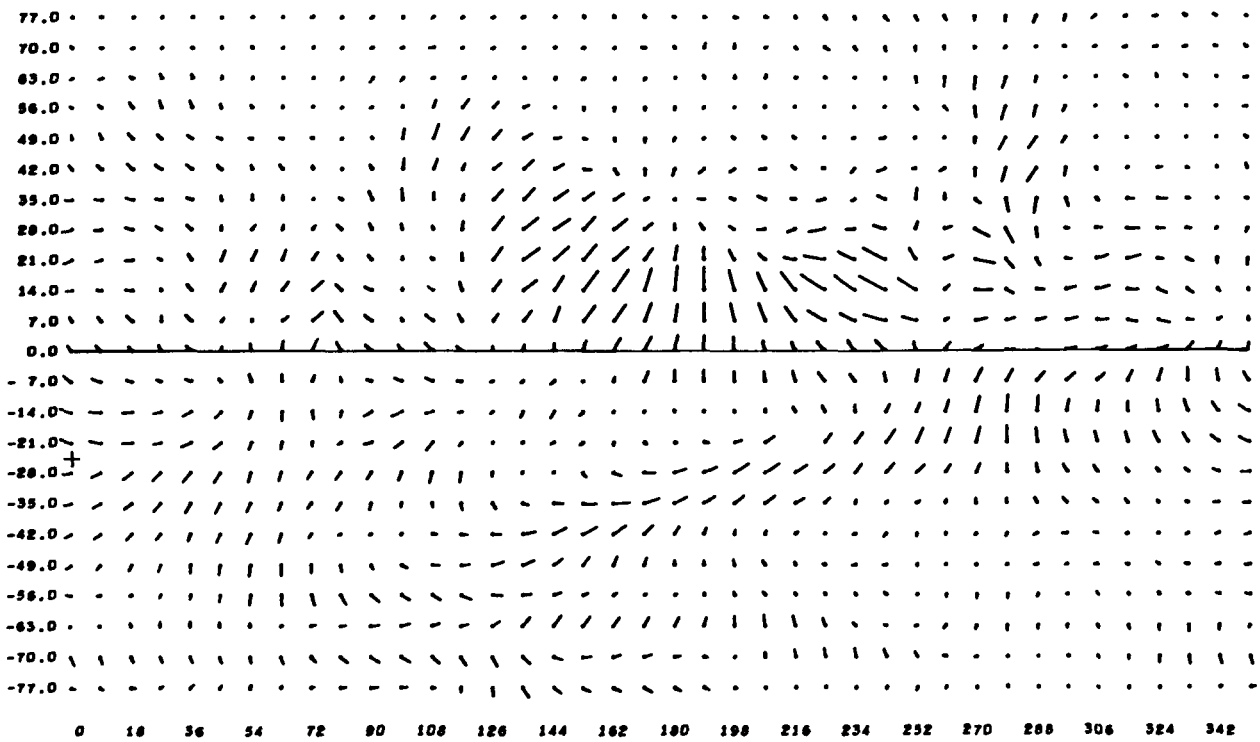

Fig. 11(a,b,c) -- "Surface" wind field for Days 18.0, 18.5, 19.0. Wind vectors are scaled against the strongest winds of 87.5 m/s in (a), 74.3 m/s in (b), and 69.8 m/s in (c).

11(b) Day 18.5

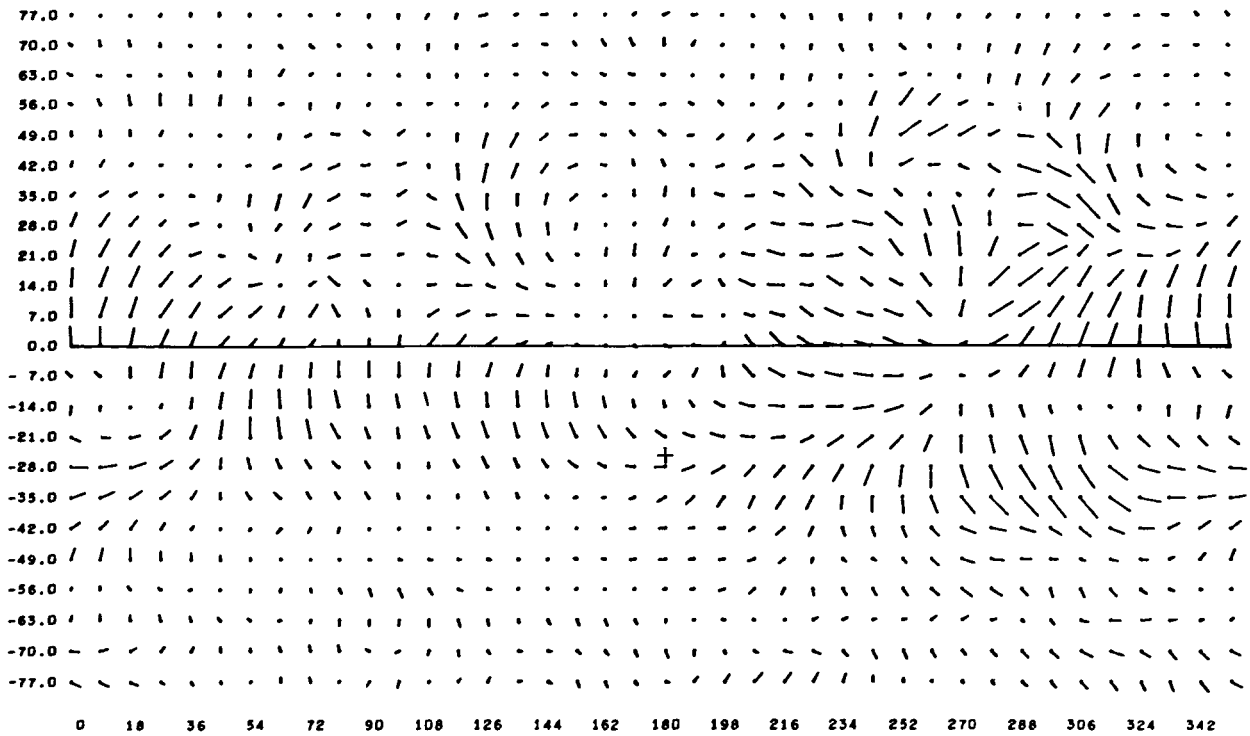

11(c) Day 19.0

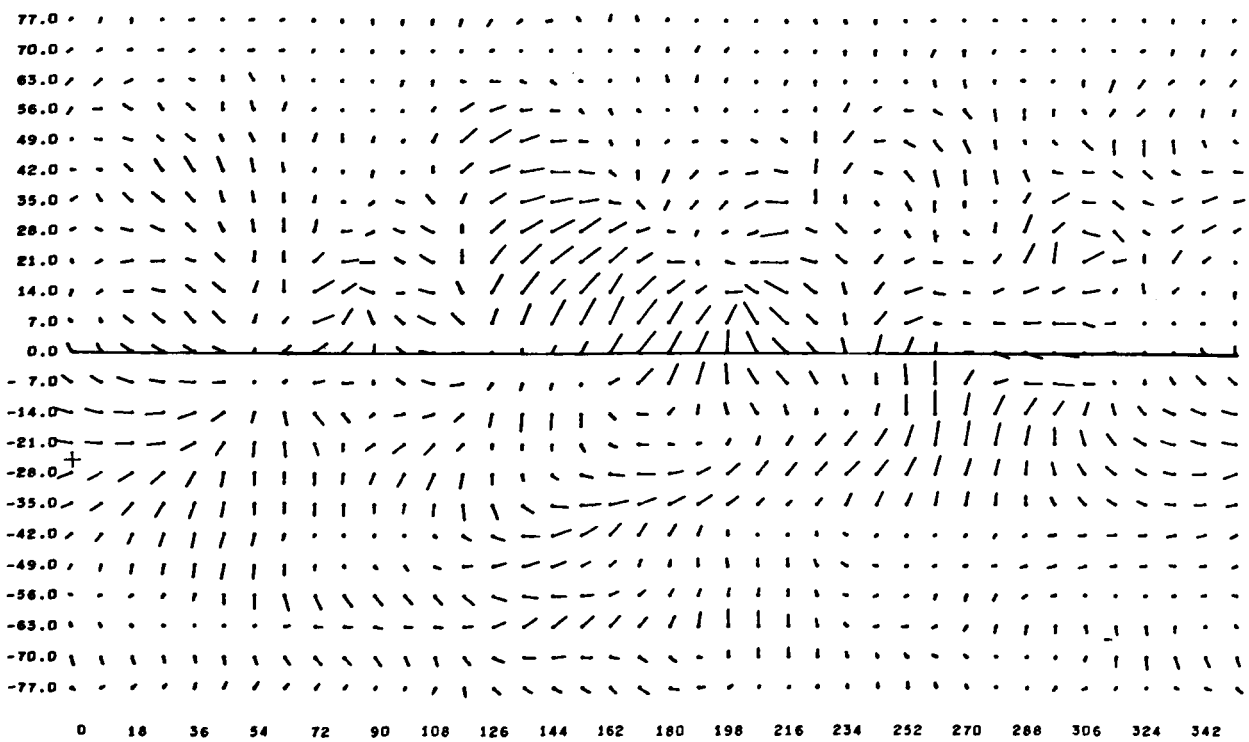

12(a) Day 18.0

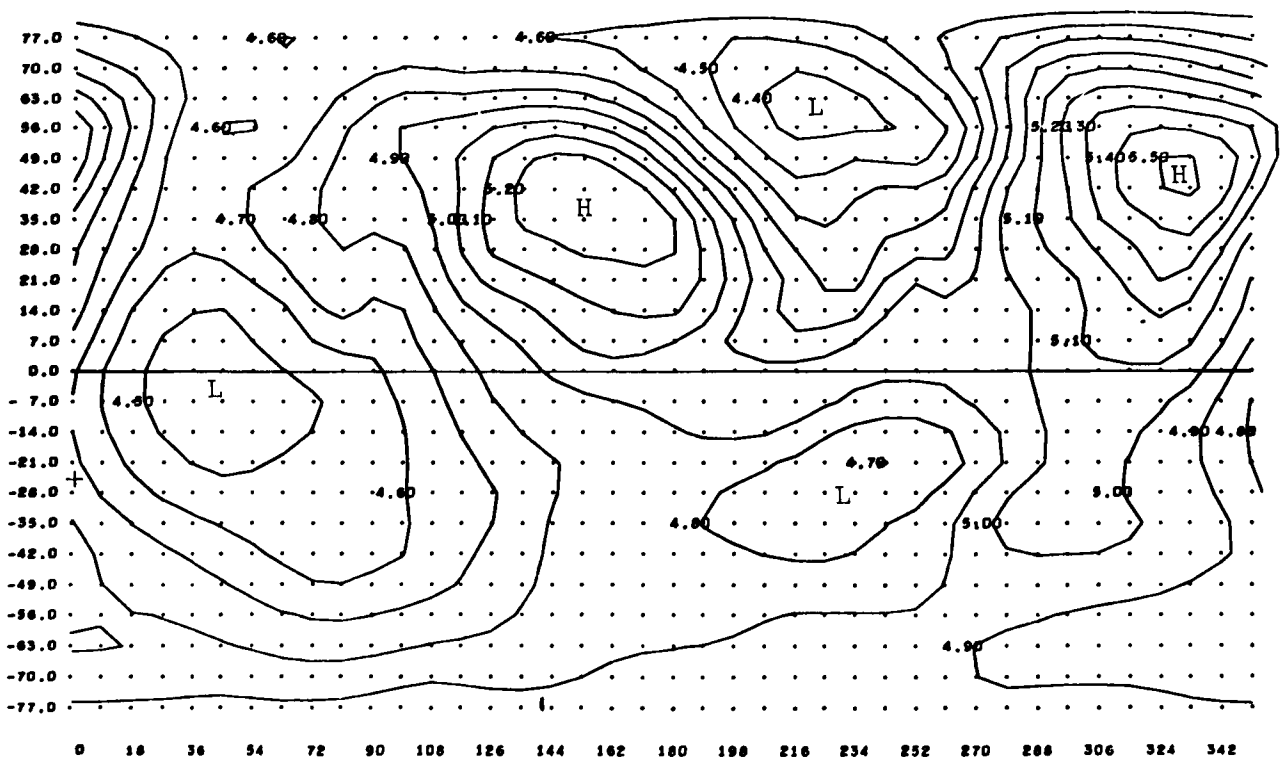

Fig. 12(a,b,c) -- Surface pressure (mb) for Days 18.0, 18.5, and 19.0.

12(b) Day 18.5

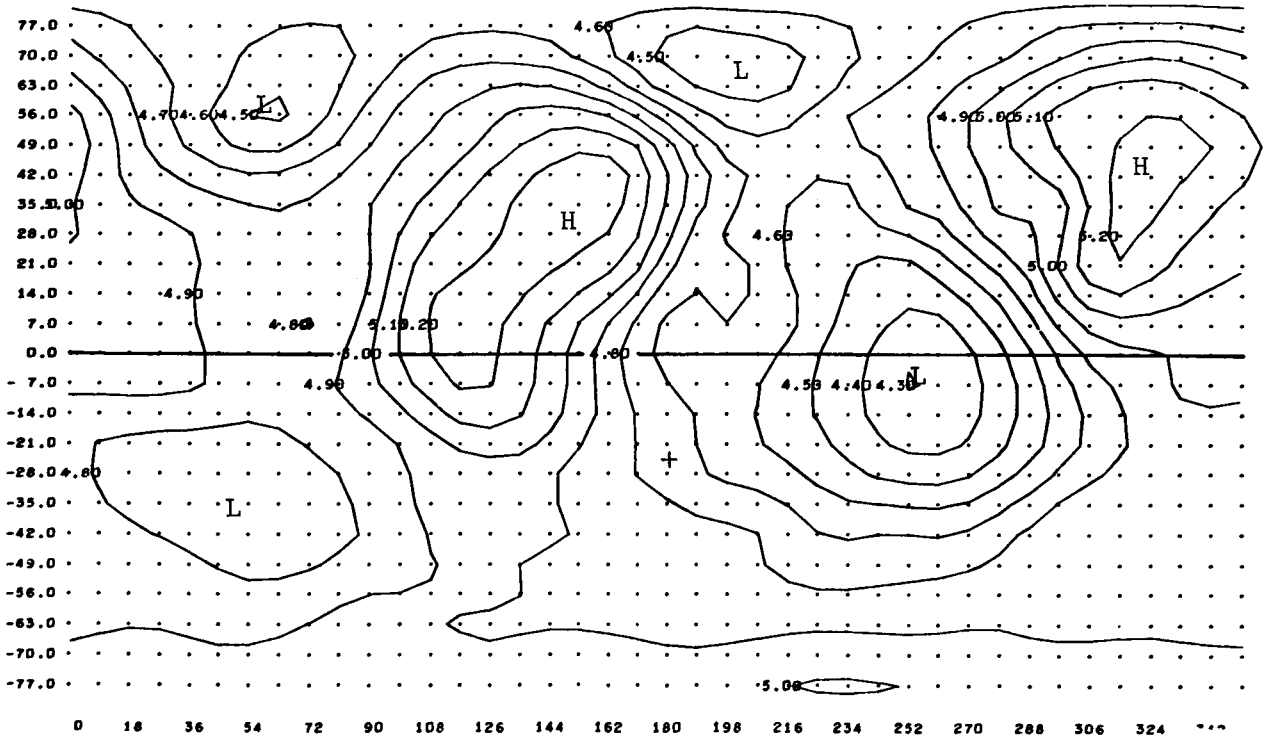

12(c) Day 19.0

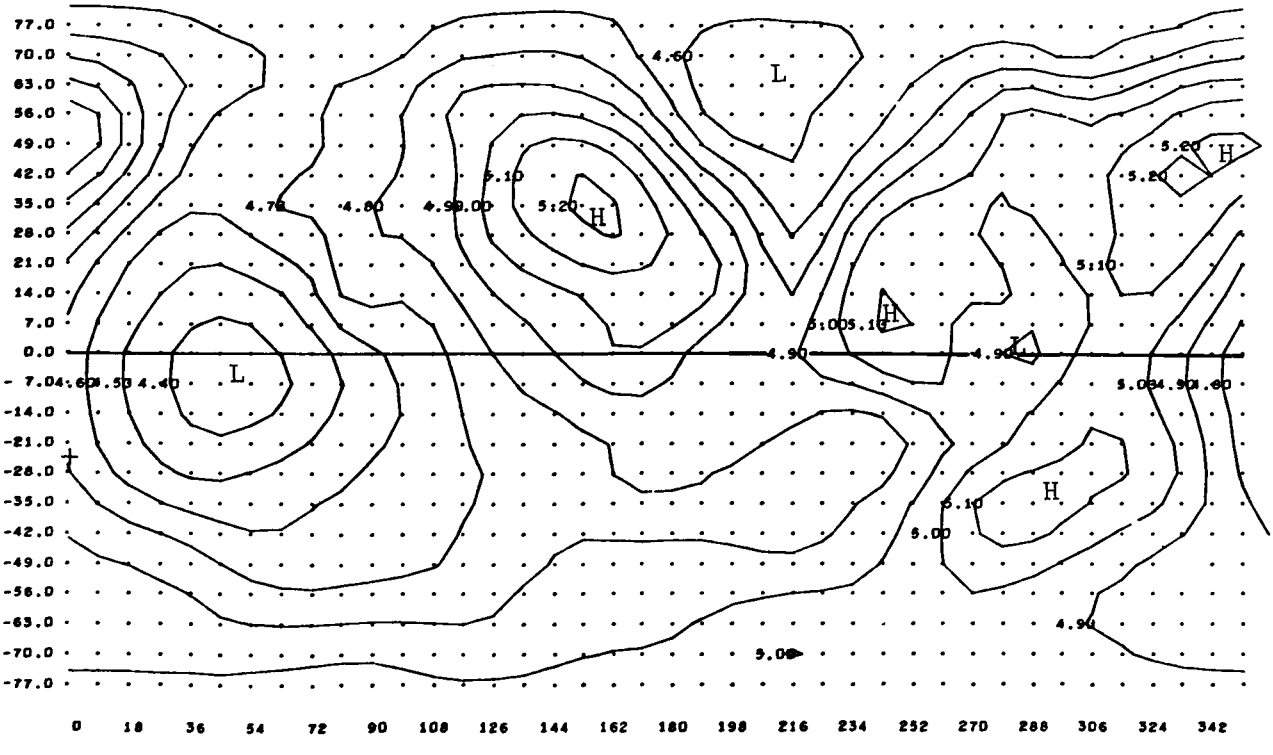

13(a) Day 18.0

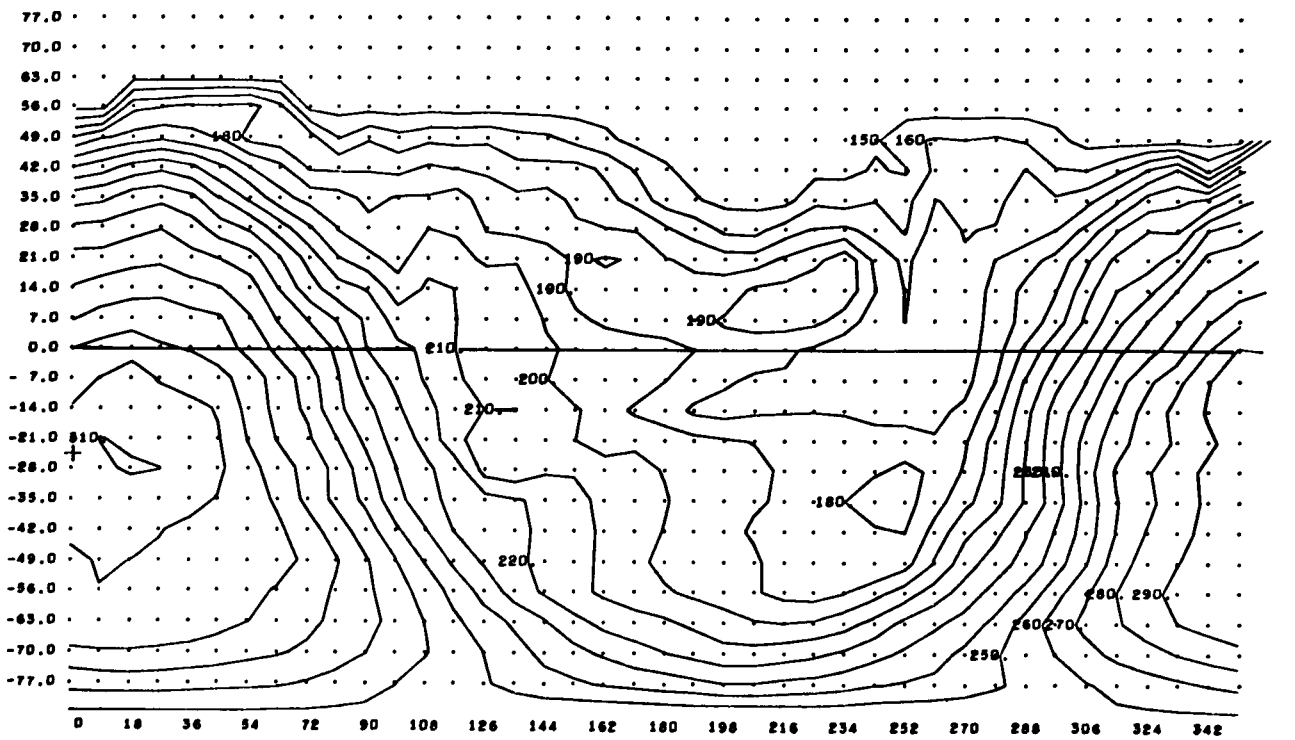

Fig. 13(a,b,c) -- Ground surface temperature (^{o}K) for Days 18.0, 18.5, and 19.0.

13(b) Day 18.5

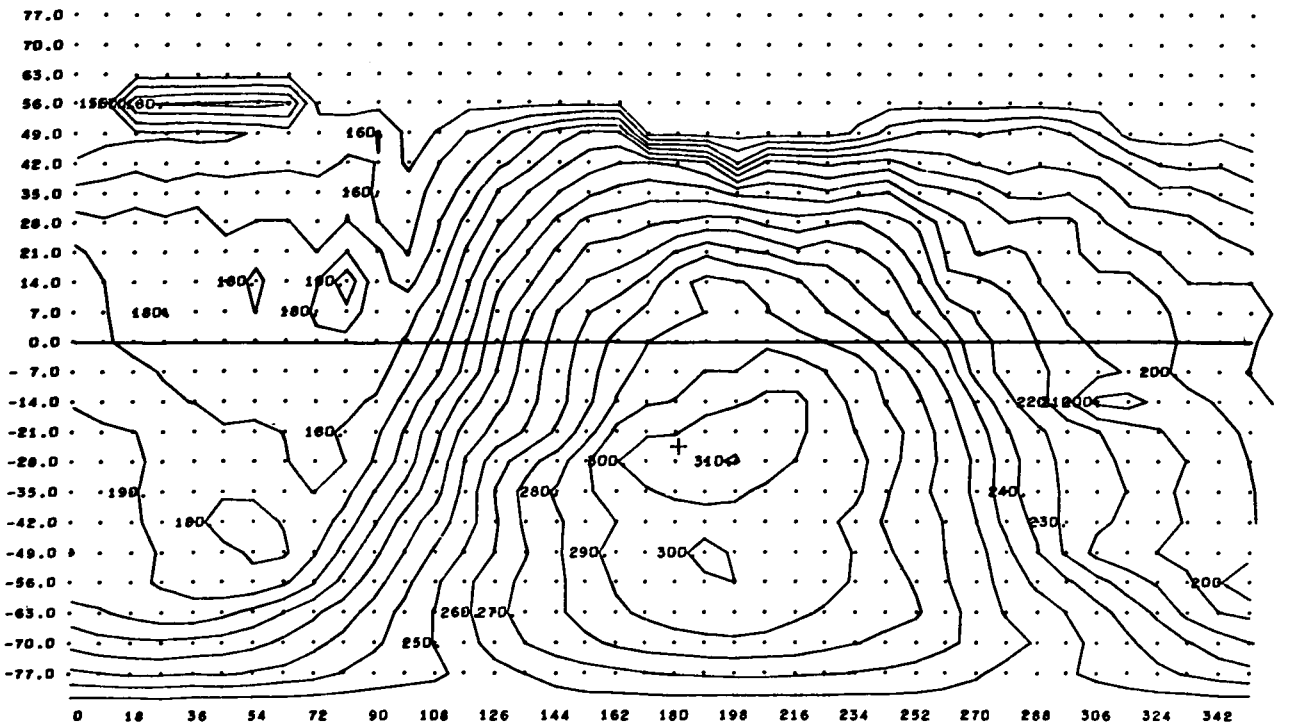

13(c) Day 19.0

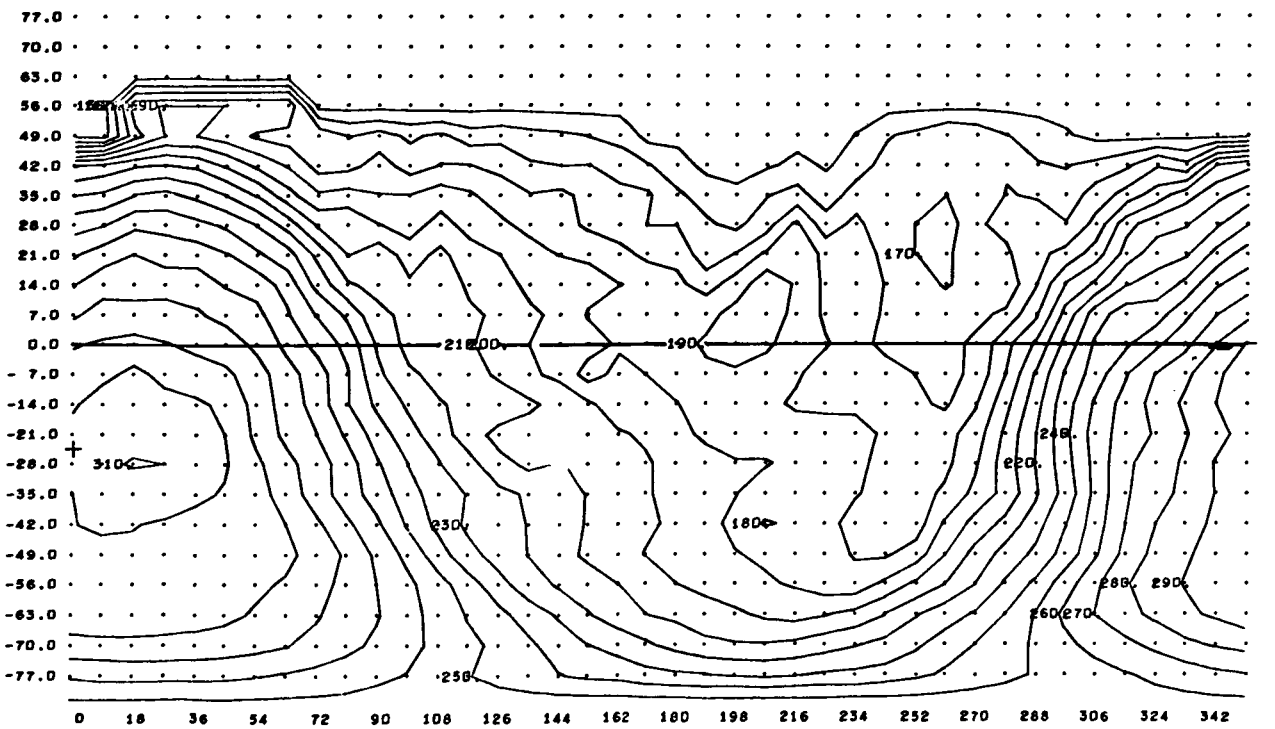

V. DISCUSSION

This study is intended to be only a brief introduction to the behavior of the current physical-dynamical model as applied to the Mars circulation. No detailed analysis of the results will be given here. Ignoring for the moment questions of shortcomings in the model, we can ask a number of interesting questions regarding these results. For example, What is the nature of the upper level waves that appear in the winter hemisphere? These disturbances have rapid growth rates initially, and their initial phase speeds correspond reasonably well with the theoretical speed for a barotropic Rossby wave (about 20 meters/sec to the east for wave number three at latitude 45°). At a later stage in their development, we see that the waves stagnate, and even retrograde in a few cases. The dominant wave number, 3, which we see on most of the maps, corresponds to the wave of maximum growth rate predicted by the linear geostrophic theory of baroclinic instability applied at latitude 45°. But these are superficial aspects, and the exact dynamical character of these waves must await a more complete inductive and deductive theoretical analysis.

The tidal motion produced by the model raises another important question. It is expected that the amplitude of the diurnal tide ought to depend strongly on the value of the surface heat exchange parameter, U_M. Although there is no reason to expect much resemblance between heat transfer over the Martian surface and heat transfer over a short grass surface on the earth, it is of interest to compare the value of U_M used in this study with the corresponding parameter that can be derived from the O'Neil data taken under unstable conditions (Lettau and Davidson, 1957). Assuming that the measured temperature at 16 meters corresponds to the surface air temperature, T_4, and extrapolating measured subsoil temperatures to the surface by means of the measured soil heat flux and thermal conductivity, one finds that the assumption is fairly well satisfied that the heat flux is proportional to the temperature difference; it exhibits only a very weak dependence on the friction veolocity, $\sqrt{|\underset{\sim}{\tau}_s|/\bar{\rho}}$. The quantity U_m derived from these data is 2 cm/sec, which is only 1/13 of the value used in the above-described Mars experiment. We have

carried out another Mars experiment, using this smaller value of V_M, as well as the smaller value, 0.003, for the thermal drag coefficient parameterizing the heat transfer under stable conditions. This new experiment ran for 8 days, starting from Day 12 of the experiment described above. The details will not be given here, inasmuch as the disturbances of the winter hemisphere circulation had not yet reached the long-term (statistical) steady state. As expected, the diurnal tide was weaker than in the first experiment, but it was still a prominent feature on the maps of the summer hemisphere and the tropics. It seems likely that the diurnal tide is an important feature of the actual Mars circulation. In addition to the usual studies of atmospheric energy transformations (see, for example, Smagorinsky, Manabe, and Holloway (1966)), it will be of some interest, in the Mars experiments, to examine the interactions between the tidal and the nontidal components of the flow.

The 6-day oscillations of energy mentioned in Section IV may be analogous to terrestrial index cycles. Study of the time variation of the energy transformations in this relatively simple atmosphere would be interesting. Similarly, the close analogy between the zonal winds at the upper level in this Mars experiment and those observed in the upper stratosphere of the earth's atmosphere suggests that detailed study of a Mars-type experiment may aid in understanding the upper stratosphere. The two regions have similar distributions of heating in the north-south direction.

There are several shortcomings in the physical model. We believe that the most serious of these are the formulation of the lower boundary conditions and the neglect of the effect of clouds and dust on the radiative heating.

We plan to reformulate the treatment of the surface stress to include a boundary layer of Ekman type. At the same time we will change the parameterization of the surface convective heat flux.

The air temperatures computed in the present experiment indicate that formation of CO_2 clouds over and near the polar caps may occasionally occur. Although we do not think that the effects of such clouds on the circulation would be important, they could be taken into account in the

model. Of greater potential significance is the possibility of the formation of water-ice clouds. These could form at higher temperatures than CO_2 clouds, and although they would be so tenuous that their latent heat effects would not be important, they could have a significant radiative effect on the surface heat balance, especially in winter in the polar region. We can think of no likely mechanism, with the possible exception of radiation from water ice clouds, that would change the conclusion that CO_2 condenses on the surface in the polar caps.

With respect to the computational instability that arose near the summer pole, an improved version of the finite difference scheme has been worked out by Arakawa (1966b) and will be available for future Mars experiments.

One possibly important item that has been neglected in the present experiment is the heat storage in the small summer-hemisphere ice cap--if this is, in fact, composed largely of CO_2. To properly handle the seasonal heat storage effects of the ice caps, one should carry the experiment through an entire Martian year. This would be costly in computer time. But because of the large radiative heating and cooling rates, the atmospheric response time is rapid, which may make it possible to simulate the Mars year adequately by accelerating the annual solar cycle by a factor of 5 or 10. We hope to try this in a future experiment.

The complete fields of the time-dependent variables have been kept on magnetic tape for every other time step (every 12 Mars minutes), and anyone interested in more detailed results is invited to communicate with the authors.

Slipher, E. C. (1962): A Photographic History of Mars, Lowell Observatory, Flagstaff, Arizona (Library of Congress Catalog No. 62-21127), 168 pp.

Smagorinsky, J., S. Manabe, and J. L. Holloway, Jr. (1965): "Numerical Results from a Nine-level General Circulation Model of the Atmosphere," Monthly Weather Rev., 93, 727-768.

REFERENCES

Arakawa, A. (1966a): "Computational Design for Long-term Numerical Integration of the Equations of Fluid Motion: Two-dimensional Incompressible Flow, Part 1," J. Computational Phys., 1, 114-143.

Arakawa, A. (1966b): "Horizontal and Vertical Differencing of the Primitive Equation Model, with σ as the Vertical Coordinate," Technical Report, Department of Meteorology, University of California at Los Angeles (in preparation).

de Vaucouleurs, G. (1964): "Geometric and Photometric Parameters of the Terrestrial Planets," Icarus, 3, 187-235.

Houghton, J. T. (1963): "The Absorption of Solar Infrared Radiation by the Lower Stratosphere," Quart. J. Roy. Meteorol. Soc., 89, 319-331.

Kaplan, L. D., G. Münch, and H. Spinrad (1964): "An Analysis of the Spectrum of Mars," Astrophys. J., 139, 1-15.

Kliore, A., et al. (1965): "Results of the First Direct Measurement of Occultation Experiment: Mars' Atmosphere and Ionosphere," Science, 149, 1243-1248.

Leovy, C. (1966): Radiative Convective Equilibrium Calculations for a Two-layer Mars Atmosphere, RM-5017-NASA, The RAND Corporation.

Lettau, H. (1959): "Wind Profile, Surface Stress and Atmospheric Drag Coefficients in the Atmospheric Surface Layer," Advances in Geophysics, 6, Atmospheric Diffusion and Air Pollution, 241-258.

Lettau, H., and B. Davidson (1957): Exploring the Atmosphere's First Mile, Vols. I and II, Pergamon Press, New York, 578 pp.

Matsuno, T. (1966a): "Integrations of the Primitive Equations by Simulated Backward Difference Method," J. Meteorol. Soc. Japan, Ser. II, 44, 76-84.

Matsuno, T. (1966b): "Scheme for Time Integrations of Oscillatory Equations with Second Order Accuracy and Sharp Cut-off for High Frequencies," J. Meteorol. Soc. Japan, Ser. II, 44, 85-88.

Mintz, Y. (1965): Very-long-term Global Integration of the Primitive Equations of Atmospheric Motion, WMO-IUGG Symposium on Research and Development Aspects of Long-range Forecasting, Geneva, WMO Technical Note No. 66, 141-167.

Phillips, N. A. (1957): "A Coordinate System Having Some Advantages for Numerical Forecasting," J. Meteorol., 14, 184-185.

Prabhakara, C. P., and J. S. Hogan, Jr. (1965): "Ozone and Carbon Dioxide Heating in the Martian Atmosphere," J. Atmospheric Sci., 22, 97-106.

Sinton, W. M., and J. Strong (1960): "Radiometric Observations of Mars," Astrophys. J., 131, 459-469.